Minireview

On uses, misuses and potential abuses of fractal analysis in zooplankton behavioral studies: A review, a critique and a few recommendations

CrossMark

Laurent Seuront

Centre National de la Recherche Scientifique, Laboratoire d'Océanologie et de Géosciences, UMR 8187 LOG, 28 avenue Foch, BP80, 62930 Wimereux, France

HIGHLIGHTS

- This work reviews uses of fractals and multifractals to zooplankton behavior.
- The basic principles behind fractal geometry are briefly rehearsed.
- Potential issues and limitations related to fractal analysis are addressed.
- Multifractals provide an objective and quantitative assessment of motion behavior.

ARTICLE INFO

ABSTRACT

Fractal analysis is increasingly used to describe, and provide further understanding to, zooplankton swimming behavior. This may be related to the fact that fractal analysis and the related fractal dimension D have the desirable properties to be independent of measurement scale and to be very sensitive to even subtle behavioral changes that may be undetectable to other behavioral variables. As early claimed by Coughlin et al. (1992), this creates "*the need for fractal analysis*" in behavioral studies, which has hence the potential to become a valuable tool in zooplankton behavioral ecology. However, this paper stresses that fractal analysis, as well as the more elaborated multifractal analysis, is also a risky business that may lead to irrelevant results, without paying extreme attention to a series of both conceptual and practical steps that are all likely to bias the results of any analysis. These biases are reviewed and exemplified on the basis of the published literature, and remedial procedures are provided not only for geometric and stochastic fractal analyses, but also for the more complicated multifractal analysis. The concept of multifractals is finally introduced as a direct, objective and quantitative tool to identify models of motion behavior, such as Brownian motion, fractional Brownian motion, ballistic motion, Lévy flight/walk and multifractal random walk. I finally briefly review the state of this emerging field in zooplankton behavioral research.

© 2015 Elsevier B.V. All rights reserved.

Contents

1. Introduction

According to the titles of several seminal monographs, such as '*The fractal geometry of Nature*' [1] and '*Fractals everywhere*' [2], fractal properties may be expected everywhere. Fractals have indeed early been suggested as a design principle in biology, as a fractal design is structurally and functionally efficient as it requires little energy to sustain itself [3]. It is hence not surprising that fractal structures have been found everywhere in nature. The Web of Science (accessed March 4, 2015) returned 23,249 and 54,024 articles respectively containing the word *fractal* in their title and topic between 1967[1] and 2015. Fractals are hence a prolific topic, and have found applications in nearly all scientific fields, including terrestrial and aquatic ecology – see Ref. [6] for a recent review – behavioral studies in general and zooplankton behavioral ecology in particular (Fig. 1).

The word plankton has first been coined by the German physiologist Viktor Hensen (1835–1924) [7] from the Greek adjective $\pi\lambda\alpha\gamma\kappa\tau\acute{o}\varsigma$ – *planktos*, wandering – to define the diverse group of organisms that live in nearly all water bodies of the planet. These organisms are essential to ocean life, as they provide a crucial source of food to many large aquatic organisms, such as fish and whales [8,9]. Plankton organisms include microbes such as viruses and bacteria (virioplankton and bacterioplankton), unicellular plants (phytoplankton) and a range of multicelled organisms (zooplankton), which mainly consists of small crustaceans as well as the eggs and larval stages of larger animals such as fish [8,9]. Most planktonic species are microscopic, but plankton also includes organisms covering a wide range of sizes, including large organisms such as jellyfish [8,9]. Though plankton organisms are typically thought to be passively drifting with currents, the quantitative assessment of the swimming behavior of even the most minute of them is increasingly thought as a critical determinant to both their ecology and their role in global biogeochemical fluxes [10–12]. Plankton behavior in general, and zooplankton behavior that is investigated in the present review, is hence a small-scale process of global significance [13]. The Web of Science (accessed March 4, 2015), however, returned a unique paper that includes the words *fractal* and *plankton* in its title, and only 42 papers include the words *fractal* and *plankton* in their topic. Similarly, only 13 papers include the words *fractal, plankton* and *behavior* in their topic. While this indicates that plankton behavioral research is still relatively poorly fractally-colored, it also stresses that fractally-inspired behavioral approaches have a significant potential to grow in the near future.

Fractals have been successfully applied to a wide range of marine biology and ecology topics including species diversity [14,15], the topographic complexity of coral reefs and rocky shores [16–22], the morphology of aquatic fauna and flora [23–33], the geometric complexity and allometric properties of marine snow [34–44], the temporal pattern of dissolved inorganic nutrients, phytoplankton and zooplankton [45–50], and the spatial distribution of both intertidal [51–59] and pelagic communities [60–68]. More specifically, fractals have been extensively used to characterize the searching behavior of organisms ranging from protozoa to large vertebrates such as seabirds, fish and mammals [6]. Note that while nearly 60% of the marine sciences studies based on fractal approaches have been published over the last decade (Fig. 1(a)),

---

[1] When Mandelbrot, the father of fractals, defined in his seminal work, entitled "*How long is the coast of Britain? Statistical self-similarity and fractional dimensions*" [4], what will formally be coined *fractal geometry* a decade later [1,5].
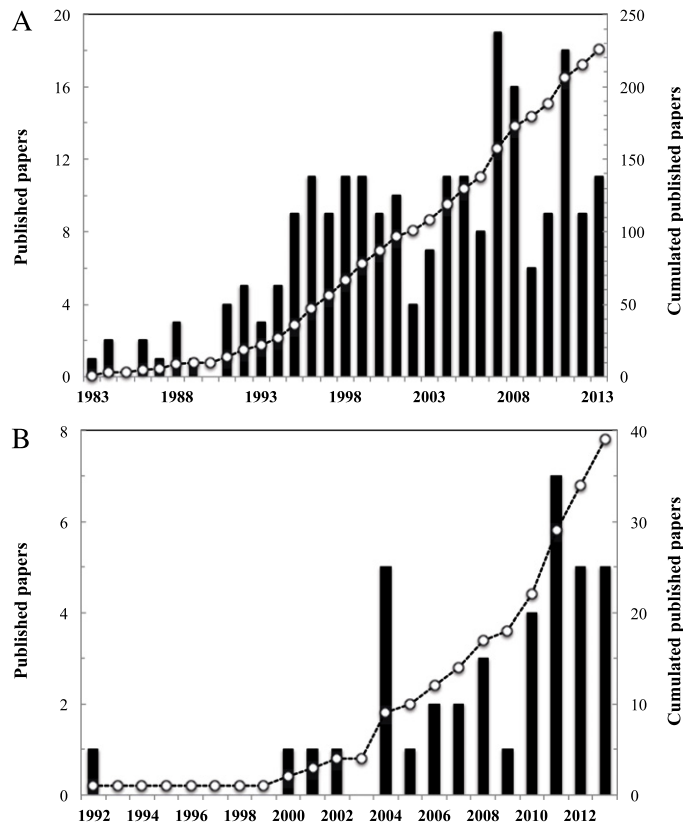
Fig. 1. Published papers that used fractal-related concepts to assess (A) the complexity of a range of patterns and processes in marine sciences and (B) the nature of zooplankton swimming behavior. The cumulated number of published papers is shown by the open dots.

the situation is far more drastic in behavioral ecology in general and in zooplankton behavioral ecology in particular as respectively nearly 80% and more than 90% of the studies based on fractal approaches have been published over the last decade (Fig. 1(b)), suggesting a field in rapid development.

Specifically, the rationale behind the increase in the use of fractal-related tools in plankton behavioral ecology lies in the fact that, in contrast to conventional behavioral metrics such as speed or turning rate, fractal analysis and the related fractal dimension D have the desirable properties to be independent of measurement scale and to be very sensitive to even subtle behavioral changes that may be undetectable to other behavioral variables [69–73]; see also Refs. [74–76] for reviews on the advantages of fractal approaches over standard metrics in behavioral science and medicine. As early claimed by Coughlin et al. [69], this creates "*the need for fractal analysis*" in behavioral studies. However, it is noteworthy that swimming trajectories of males, females and non-ovigerous females of the estuarine copepod *Pseudodiaptomus annandalei* that are unambiguously distinct through visual inspections – see e.g. Ref. [77], their Fig. 8 – and respectively described as "*predominantly rectilinear*", "*more convoluted*" and "*more tortuous*" (hence putatively fulfilling different degrees of space-filling) were characterized by non-significantly different fractal dimensions [77]. Similar conclusions were reached for the swimming behavior of *Euterpina acutifrons* females despite the visual differences observed in the complexity of their trajectories (Wasserman, personal communication; see also Ref. [78], their Fig. 1). These facts may suggest that fractals are not necessarily the ultimate tool to assess the complexity of swimming behavior under any experimental or environmental conditions.

Despite the ever increasing number of publications that used fractals to answer key questions in aquatic biology and ecology (Fig. 1; see also Ref. [6] for a recent review), the significance of the seminal work of Mandelbrot [1,4,5] may still have to reach many biologists and ecologists, as according to the Web of Science (accessed March 4, 2015) the research areas related to *Marine and Freshwater Biology, Oceanography*, and *Water Resources* account for only ca. 0.5% and 1.4% of the published articles containing respectively the word *fractal* in their title and topic. As such, the inappropriate use of fractal analysis in ecology in general, and in behavioral ecology in particular – though not an isolated case, see e.g. Refs. [67,79–88] – may have critical consequences on the development of this research area. For instance, a few studies conducted on the swimming behavior of a range of zooplankton species explicitly reported fractal dimensions falling outside the theoretical range $1 \leq D \leq 2$ expected for a swimming trajectory, i.e. $D < 1$ [77,89] and $D > 2$ [69,90]. In the absence of both a detailed procedure related to the way they conduct their fractal analysis and a discussion of this aspect, this might indicate potential
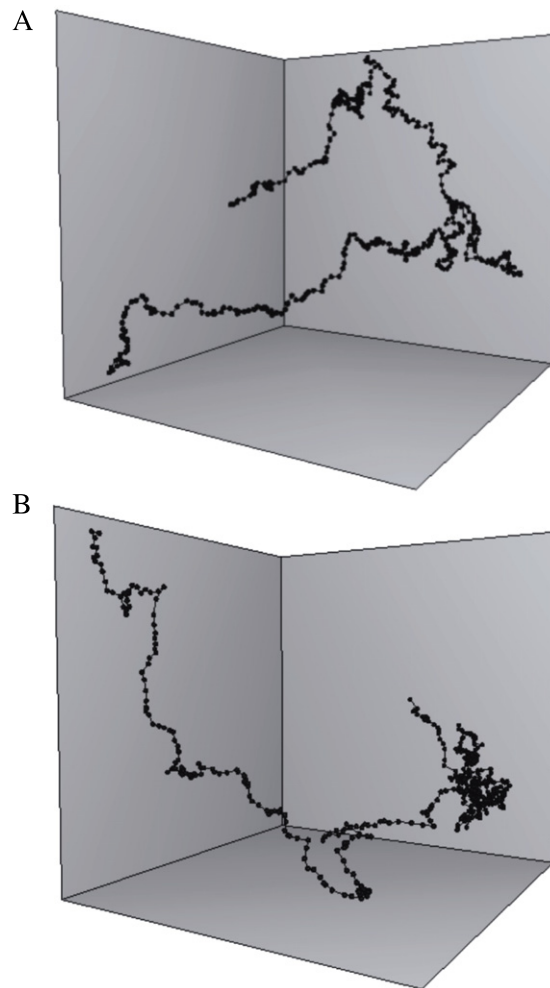
Fig. 2. Representative three-dimensional trajectories of *E. affinis* males (A) and non-ovigerous females (B). Each trajectory has been plotted in a standardized volume of 15 cm × 15 cm × 15 cm.
Source: Modified from Ref. [105].

flaws in their approach. These flaws are difficult to unambiguously assess, but may stem from a range of factors that are both extrinsic and intrinsic to fractal analysis such as the potential anisotropy and different lengths of the analyzed trajectories, and the goodness-of-fit used to characterize the range of scale over which the scaling properties of the trajectories (hence their fractal dimensions) is estimated.

In this context, and considering the rapid expansion of the applications of fractal-related methods to zooplankton swimming behavior (Fig. 1(b)), it is now a critical time to review the potential issues and limitations that may hamper the future development of this burgeoning field. In this context, I first briefly rehearse some of the basic principles behind fractal geometry before consideration of its use in behavioral ecology. I subsequently address potential issues and limitations related to fractal analysis that may lead to spurious results and conclusions, hence I suggest a few critical steps, criteria and remedial procedures that need to be addressed for a behavioral fractal analysis to be meaningful. After addressing the fundamental differences between self-similar and self-affine fractals, I describe one of the most widely used techniques to characterize self-affine fractals, and also how fractal dimensions can be derived from frequency distribution. I subsequently introduce the concept of multifractals, and describe how multifractals uniquely provide a direct, objective and quantitative tool to thoroughly identify models of motion behavior, such as Brownian motion (i.e. normal diffusion), fractional Brownian motion, ballistic motion, Lévy flight/walk and multifractal random walk. I finally briefly review the state of this emerging field in zooplankton behavioral research.

To make the point that the issues that I discuss in this paper are current, I chose to critically assess 44 papers published since 1992 in which the spatial and/or temporal complexity of zooplankton swimming behavior were analyzed using fractal-related tools (Tables 1–3). Note, however, that any of the theoretical and practical limitations of fractal analysis addressed here are quite ancillary to the main point of these papers – most of them use fractal analysis as a tool to compare swimming trajectories, or more generally swimming behaviors, between experimental conditions rather than to determine the true

Table 1
Review of zooplankton behavioral studies based on self-similar fractal methods.

Organism	Species	Method	Scaling range	Optimization criteria	Fractal dimension	2D vs. 3D	Source
Fish	Clownfish (*Amphiprion perideraion*)	$L(l) \approx l^{1-D}$	63.1[a]	na	$D > 2$	3D	[69][b]
Fish	Barramundi (*Lates calcarifer*)	$L(l) \approx l^{1-D}$	na	na	$D < 1$	2D	[89][b]
Crustacean (Cladocera)	*Daphnia magna*	$N(l) \approx l^{-D}$	7.5[a]	na	$D > 2$	2D	[90][b]
Crustacean (Cladocera)	*D. pulex*	$N(l) \approx l^{-D}$ $L(l) \approx l^{1-D}$	6.3	R^2-SSR; zero-slope	$1 \leq D \leq 2$	3D	[91]
Crustacean (Copepoda)	*O. venusta*	$N(l) \approx l^{-D}$ $L(l) \approx l^{1-D}$	200	R^2-SSR	$1 \leq D \leq 2$	2D	[92]
Crustacean (Cladocera)	*Daphnia pulicaria*	$L(l) \approx l^{1-D}$	na	na	$1 \leq D \leq 2$	2D	[93]
Crustacean (Copepoda)	*T. longicornis*	$L(l) \approx l^{1-D}$	na	na	$1 \leq D \leq 2$	2D	
Crustacean (Cladocera)	*D. pulex*	$N(l) \approx l^{-D}$	100[a]	r^2	$1 \leq D \leq 2$	3D	[94]
Simulation of swimming tracks	–		na	na		3D	
Crustacean (Copepoda)	*E. affinis*	$N(l) \approx l^{-D}$	na	r^2	$1 \leq D \leq 2$	2D	[95]
Crustacean (Cladocera)	*D. pulex*	$N(l) \approx l^{-D}$	100[a]	r^2	$1 \leq D \leq 2$	3D	[96]
Simulated trajectories	–	$N(l) \approx l^{-D}$	100[a]	r^2		3D	
Crustacean (Copepoda)	*Leptodiaptomus ashlandi*	$N(l) \approx l^{-D}$	100[a]	r^2	$1 \leq D \leq 2$	3D	[97]
Crustacean (Copepoda)	*C. furcatus*	$N(l) \approx l^{-D}$	na	na	$1 \leq D \leq 2$	2D	[98]
Fish	Whitefish (*C. lavaretus*)	$N(l) \approx l^{-D}$	5[a]	r^2	$1 \leq D \leq 2$	2D	[99]
Crustacean (Copepoda)	*T. longicornis*	$N(l) \approx l^{-D}$ $L(l) \approx l^{1-D}$	na	R^2-SSR	$1 \leq D \leq 2$	2D	[71]
Simulated trajectories	–		na	r^2	$1 \leq D \leq 2$	3D	[100]
Crustacean (Copepoda)	*A. clausi, C. typicus, P. parvus, P. elongatus, T. longicornis*	$L(l) \approx l^{1-D}$	na	r^2	$1 \leq D \leq 2$	3D	[72]
Crustacean (Copepoda)	*T. longicornis*	$N(l) \approx l^{-D}$	na	na	$1 \leq D \leq 2$	3D	[101]
Crustacean (Cladocera)	*D. pulicaria*	$N(l) \approx l^{-D}$	na	r^2	$1 \leq D \leq 2$	2D	[102]
Fish	Malabar grouper (*E. malabaricus*)	$N(l) \approx l^{-D}$	na	r^2	$1 \leq D \leq 2$	3D	[103]
Crustacean (Copepoda)	*E. affinis*	$N(l) \approx l^{-D}$ $m(l) \approx l^{-D}$	na	R^2-SSR	$1 \leq D \leq 2$	3D	[73]
Crustacean (Copepoda)	*P. annandalei*	$N(l) \approx l^{-D}$	na	na	$D < 1$	2D	[77][b]
Crustacean (Copepoda)	*E. affinis*	$N(l) \approx l^{-D}$	na	na	$1 \leq D \leq 2$	3D	[104][c]
Crustacean (Copepoda)	*E. affinis*	$N(l) \approx l^{-D}\ m(l) \approx l^{-D}$	na	R^2-SSR	$1 \leq D \leq 2$	3D	[105]
Crustacean (Copepoda)	*L. branchialis*	$N(l) \approx l^{-D}$	na	na	$1 \leq D \leq 2$	3D	[106][c]
Crustacean (Copepoda)	*E. acutifrons*	$N(l) \approx l^{-D}$	ca. 10 000[a]	r^2	$1 \leq D \leq 2$	3D	[78]

[a] The scaling ranges were not explicitly provided, but estimated graphically from the figures of the published work.

[b] These references unambiguously reported fractal dimensions that fall outside the theoretical range $1 \leq D \leq 2$ expected for a swimming trajectory.

[c] The confidence intervals estimated for fractal dimensions from the means and standard deviations provided in both Table 2 of Ref. [104] and Fig. 4(d) of Ref. [106] suggest that a few fractal dimensions fall outside the range $1 \leq D \leq 2$, in particular with $D < 1$.

value of their fractal dimensions – hence the criticisms implied by the following statements and analyses do no detract from the central point of their work.

2. Fractal geometry in a (very) few words

In a paper entitled '*How long is the coast of Britain? Statistical self-similarity and fractional dimensions*', Mandelbrot [4] defined the basis of what will be formally coined *fractal geometry* a decade later [1,5], and introduced a new concept that has rapidly provided a unifying and cross-disciplinary basis for the description of nature's complexity [2,6,14,123–127]. Many natural phenomena have a nested irregularity and may look similarly complex under different resolution. For instance, the complexity of coastlines will repeatedly become evident if a section of that coastline is studied in finer and finer detail, ultimately until the outlines of individual boulders, rocks, and grains of silt and sand are being traced. A fundamental consequence of this nested structure is that the length of a coastline, or the surface of any two-dimensional fractal structure,

Table 2
Review of zooplankton behavioral studies based on self-affine fractal methods.

Organism	Species	Method	Scaling range	Optimization criteria	2D vs. 3D	Source
Crustacean (Copepoda)	*D. pulex*	$E(f) \approx f^{-\beta}$	na	na	3D	[107]
Crustacean (Copepoda)	*C. darwini*	$p(t) \approx t^{-c}$	6–7[a]	na	2D	[108]
Crustacean (Copepoda)	*C. hamatus*	$P(t \leq T) \approx t^{-\phi}$	33.3[a]	R^2-SSR	3D	[70]
Crustacean (Copepoda)	*C. furcatus*	$E(f) \approx f^{-\beta}$	na	na	3D	[98]
Crustacean (Copepoda)	*P. annandalei*	$E(f) \approx f^{-\beta}$	100[a]	R^2-SSR	2D	[109]
		$p(t) \approx t^{-c}$	na	r^2		
		$p(v) \approx v^{-c}$[b]	–	–		
Crustacean (Copepoda)	*E. affinis*	$p(v) \approx v^{-c}$	15[a]	r^2	2D	[110]
		$p(t) \approx t^{-c}$	na	r^2		
Crustacean (Copepoda)	*E. affinis*	$p(t) \approx t^{-c}$	2.5–27[a]	na	2D	[111]
Crustacean (Copepoda)	*P. annandalei*	$p(t) \approx t^{-c}$	10–100[a]	r^2	2D/3D	[112]
		$p(v) \approx v^{-c}$[b]	–	–		
	E. affinis	$p(t) \approx t^{-c}$	10–100[a]	r^2	2D/3D	[112]
		$p(v) \approx v^{-c}$[b]	–	–		
Crustacean (Copepoda)	*P. annandalei*	$p(v) \approx v^{-c}$[b]	–	–	3D	[113]
Crustacean (Copepoda)	*A. clausi, C. typicus, P. parvus, P. elongatus, T. longicornis*	$N(l \leq L) \approx l^{-\phi}$	13–20[a]	r^2	3D	[72]
Crustacean (Copepoda)	*E. affinis*	$p(v) \approx v^{-c}$[b]	–	–	2D	[114]
Crustacean (Copepoda)	*C. sinicus*	$p(v) \approx v^{-c}$[b]	–	–	2D	[115]
Crustacean (Copepoda)	*T. longicornis*	$E(f) \approx f^{-\beta}$	10–100[a]	na	2D	[116]
		$p(v) \approx v^{-c}$[b]	–	–		
Crustacean (Copepoda)	*E. affinis*	$N(l \leq L) \approx l^{-\phi}$	na	R^2-SSR	3D	[73]
Crustacean (Copepoda)	*P. annandalei*	$p(v) \approx v^{-c}$[b]	–	–	3D	[77]
Crustacean (Copepoda)	*C. furcatus*	$E(f) \approx f^{-\beta}$[c]	–	–	3D	[117]
Crustacean (Copepoda)	*T. longicornis*	$p(v) \approx v^{-c}$[b]	–	–	2D	[118]
Crustacean (Copepoda)	*E. affinis*	$p(v) \approx v^{-c}$[b]	–	–	3D	[119]
Crustacean (Copepoda)	*L. branchialis*	$p(v) \approx v^{-c}$[b]	–	–	3D	[106]
Crustacean (Copepoda)		$p(t) \approx t^{-c}$	na	r^2	3D	
Crustacean (Copepoda)	*E. affinis*	$p(v) \approx v^{-c}$[b]	10–100[a]	r^2	2D	[120]
Crustacean (Copepoda)	*P. annandalei*	$p(v) \approx v^{-c}$[b]	–	–	3D	[104]
Crustacean (Copepoda)	*P. marinus*	$p(t) \approx t^{-c}$[b]	–	–	2D	[121]
Crustacean (Copepoda)		$p(v) \approx v^{-c}$[b]	–	–	2D	

[a] The scaling ranges were not explicitly provided, but estimated graphically from the figures of the published work.
[b] The probability density functions $p(v)$ and $p(t)$ of instantaneous velocity v and residence time t in a behavioral state were not used to infer the scaling properties of velocity or residence time fluctuations, but to assess eventual differences in the shape of a log–log plot of $p(v)$ vs. v and $p(t)$ vs. t between different experimental conditions.
[c] Spectral analysis was not used to assess the nature of the scaling and estimate the exponent β, but instead to define an eventual characteristic time from the velocity data of swimming trajectories.

does not converge to a fixed value, but keeps increasing, *theoretically* without any upper limit. Coastlines do not have a length; instead, they have *fractal extents*, and common statements such as "*the length of coastline of Great Britain plus its principal islands is about 19,491 miles*" [128] are fundamentally flawed. The nested structure of fractal objects, referred to as scale-invariant or self-similar (i.e. each portion can be considered a reduced-scale image of the whole), could be thought of as an additional source of complexity; in contrast to Euclidean lines, they cannot be differentiated or integrated, hence they are impervious to calculus. A nested structure, however, potentially becomes a source of simplicity in the framework of fractal geometry, where the degree of complexity of a given pattern or process can be described by a dimension *D*, the so-called fractal dimension. In contrast to conventional (Euclidean) dimensions, a fractal dimension is fractional, hence describes the degree of complexity and tortuosity of an object. For instance, the Euclidean dimensions, *d*, of a straight line, a circle and a cube are respectively $d = 1$, $d = 2$ and $d = 3$. A fractal line will have a fractal dimension $1 \leq D \leq 2$, and a completely self-similar complex surface will ultimately lead to $D = 3$. For example, the UK coastline has a fractal dimension of 1.27 [4], and a typical cloud outline has a fractal dimension $D = 1.35$ [129]. Two of the more complex living objects reported so far are the multiply branched, fine filamentous seaweed *Desmarestia menziesii* which has a fractal dimension *D* bounded between 1.51 and 1.83 [28] and the ramified sponge *Raspailia inaequalis* which has *D* bounded between 1.44 and 1.75 [30].

3. Fractal geometry and zooplankton swimming behavior

3.1. From scale-dependent to scale-independent behavioral metrics

Standard behavioral metrics such as trajectory length, move length, move duration, swimming speed, turning angle, turning rate, and net displacement are implicitly a function of their measurement scale [91]. This scale-dependence implies that there is no single scale at which swimming trajectories can be unambiguously described. This is not the case, however, for fractal dimensions. The fractal dimension *D*, considered as a scale-independent descriptor of swimming behavior, is

bounded between $D = 1$ and $D = 2$. When an organism moves along a completely linear path, the actual distance traveled equals the displacement between the start and the finish, and $D = 1$. In the opposite extreme instance of curviness, when the motions are so complex that the path fills the whole available space, $D = 2$.

3.2. On the boundaries of the fractal dimensions of swimming trajectories

I address the *a priori* paradoxical result that fractal dimensions estimated from three-dimensional trajectories are smaller than 2, the expected lower bound for objects embedded in a three-dimensional space [130]. An object embedded in a *d*-dimensional space is expected to have a fractal dimension bounded between $d − 1$ and d [126]. This is indeed the case for many natural objects. For instance, a succession of dust particles spread out linearly will have a dimension bounded between 0 and 1 as they occupy a fraction of the space greater than a single point (dimension 0), and lower than a line (dimension 1). Similarly, a convoluted curve will occupy a fraction of space between a line (dimension 1) and a surface (dimension 2). In contrast, the dimension of any three-dimensional branching structure such as trees and marine sponges will be bounded between 2 (a surface) and 3 (a volume). The swimming trajectories of zooplankton organisms are typically embedded in a three-dimensional environment (Fig. 2). However, each change of direction occurring within a two-dimensional space, the trajectory of any zooplankton organism remains a convoluted two-dimensional object. Its fractal dimension is bounded between a one-dimensional space (i.e. a line, $D = 1$) and a two-dimensional space (i.e. a surface, $D = 2$); see Ref. [6] for examples and a detailed discussion. A direct consequence of the above-mentioned property is to question previous reports of fractal dimensions falling beyond the limits discussed above for both two-dimensional analyses ($D < 1$ [89]) and ($D > 2$ [90]), and three-dimensional analyses ($D > 2$, [69]), and $D < 1$, [77]. Note that this issue is not limited to plankton behavioral ecology as fractal dimensions $D < 1$ and $D > 2$ have respectively been found for the trajectories of the sandy shore snail *Batillaria zonalis* [131] and the Gray wolf *Canis lupus* [132].

It is also noteworthy that, as defined above, a trajectory corresponds to the continuous curve drawn from the line segments joining successive positions recorded in time. This fundamentally differs from the discrete point pattern created by the successive locations occupied by the organism in time. In the former case, $1 \leq D \leq 2$, while in the latter $0 \leq D \leq 1$. As a consequence, the fractal dimension of the trajectory followed by a swimming organism *does not* equal the fractal dimension of its successive positions, especially when the spatial resolution of the measurements is large compared to the size of the organism; this is typically the case in zooplankton when sudden accelerations and strong jumps occur (up to hundreds of mm s^{-1} for a millimeter-scale zooplankton organism, see e.g. Ref. [133]) and lead to 'positional gaps' that require specific technologies such as high-speed imaging to be resolved [133].

Finally, it is undeniable that the fundamental aspiration of behavioral studies using fractal-related tools lies in the comparison and understanding of e.g. "*the geometry of trajectories between*" experimental and environmental "*conditions rather than to determine the true value of their fractal dimension*" [77]. However, the colloquialisms "*the proof is in the numbers*" and "*numbers don't lie*" have strong, and undisputable, implications in Science. For instance, Sir Isaac Newton's Universal Law of Gravitation put an upper limit to the size of animals, which is fundamentally restricted by both the strength of bone and the mass of the Earth [134–138]. In other words, an elephant *could not* fly and a whale *could not* walk even if they had wings and legs. Similarly, fractal dimensions estimated from the trajectory of a swimming organism – and more generally from any convoluted line [4] – have indefectible lower and upper limits that *cannot* be exceeded to ensure the relevance of the conclusions of any fractal analysis, whatever the biological and ecological questions driving the analysis may be. To paraphrase Sir William Huxley, this is essential to avoid one "*great tragedy of Science, the slaying of a beautiful hypothesis by an ugly fact*" [139].

As explored below, the discrepancies observed between empirical fractal dimensions and their theoretical limits might result from (i) the lack of objective procedures to identify the scaling ranges, and the subsequent fractal dimensions of swimming trajectories, and (ii) neglecting to take into account the potential anisotropy of the swimming trajectories.

4. Estimating the fractal dimensions of swimming trajectories

4.1. The box-counting method

To unambiguously address the issues of estimating the fractal dimension D from "*the slope of the power fit of the log–log plot of the number of boxes vs. mesh size*" [77], let us first briefly recall the reader not acquainted with fractal analysis the basic principles of the box-counting method, one of the most widely used methods to characterize the geometric complexity of swimming trajectories (i.e. 19 of the 24 papers reviewed here used the box-counting method, either alone or in conjunction with another method, to estimate the fractal dimensions of swimming trajectories; see Table 1). This method relies on the *l* cover of an object, i.e. the number of boxes of length *l* required to cover the object. Practically, this method superimposes a regular grid of boxes of length *l* on the object and counts the number of occupied boxes. This procedure is repeated using different values of *l*. The volume occupied by a swimming trajectory is then estimated using a series of boxes spanning a range of volumes down to some small fraction of the entire volume, typically the size of the organism considered. The number of occupied boxes increases with decreasing box size, leading to the following power-law relationship:
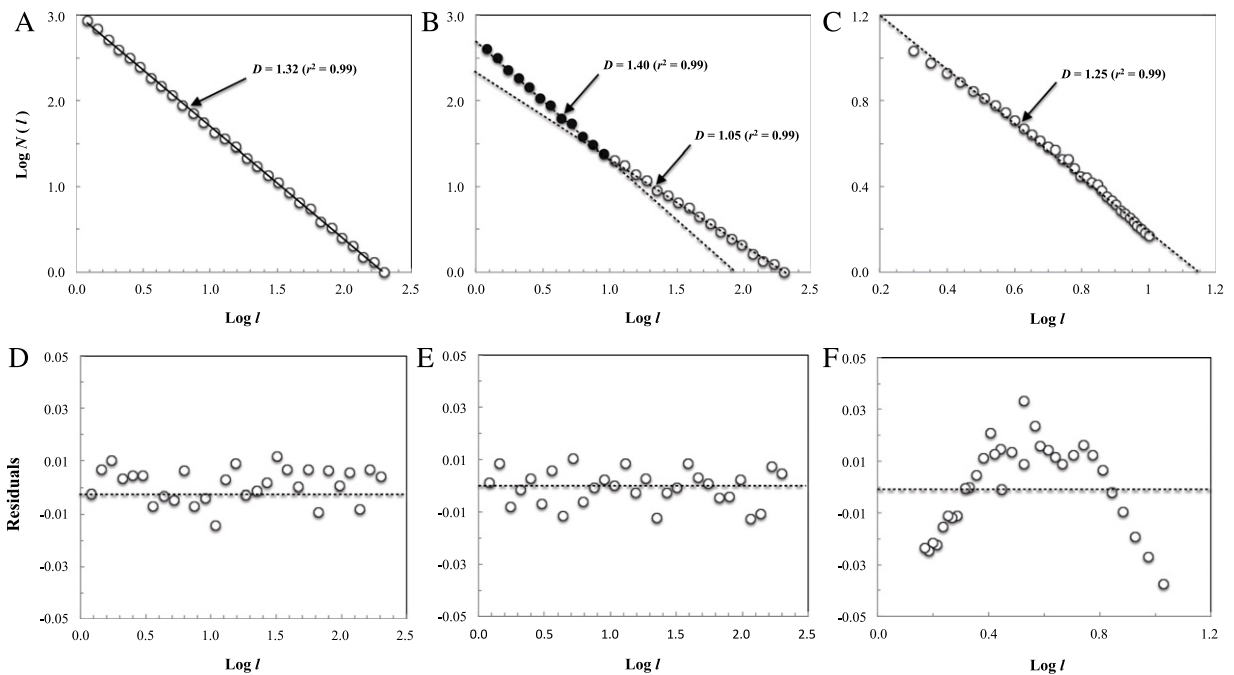
$$N(l) \propto l^{-D_b} \tag{1}$$

Fig. 3. Log–log plots of $N(l)$ vs. l for *O. venusta* (A, B) and *C. lavaretus* (C). The data used in (A, B) were originally published by Seuront et al. [92] in their Figs. 7 and 8, and the data used in (C) were digitized from the Fig. 4 of Mahjoub et al. [99] using GraphClick (Arizona Software).

where l is the box size, $N(l)$ is the number of boxes occupied by the swimming trajectory, and D_b is the box fractal dimension; D_b is estimated from the slope of the linear trend of the log–log plot of $N(l)$ vs. l. While this may seem straightforward and easily achievable through the implementation of an automated fitting procedure using any programming languages, a few potential biases nevertheless need to be considered to achieve a meaningful and sound analysis.

4.2. When is a 'linear' log–log plot actually linear?

4.2.1. Significant linear regressions do not always imply linearity

When dealing with exact fractals, there are no difficulties in calculating a fractal dimension. The log–log plots are fundamentally linear and an expected and *a priori* known result is always recovered whatever the methods employed. However, when dealing with patterns and processes whose properties are not known *a priori* (e.g. coastlines, swimming trajectories), complications begin to arise. In particular, if the box size is small compared to the resolution of the object considered, the log–log plot of $N(l)$ vs. l will artificially become flatter; in contrast, box size too large for the size of the object will artificially lead to increase the slope of log $N(l)$ vs. log l [4]; see also Refs. [32,91] for biological applications to the marine environment.

Most previous studies that used fractal tools to assess the complexity of zooplankton swimming trajectories seem to have implicitly made an assumption of linearity in log–log plots, as 37.5% of the 24 studies investigated here (Table 1) do not mention the use of any criteria of fitting quality, 41.7% used linear regression and the coefficient of determination r^2, and 20.8% used one (or more) objective optimization procedures. This suggests that scaling ranges may have been estimated rather subjectively, and their relevance relies on the statistical significativity of the coefficient of determination (r^2). Ensuring the significativity of the coefficient of determination (r^2) is, however, far from being sufficient to conclude to the presence of fractality; see Refs. [6,67,79–84] for reviews on various aspects of this issue, and [85–88] for examples of overturned conclusions of previously claimed fractal properties. This issue is further illustrated using two examples of fractal properties identified in the swimming behavior of the copepod *Oncaea venusta* [92] and the larvae of the European whitefish *Coregonus lavaretus* [99]. Note that these two studies have been specifically chosen as the scaling ranges used to estimate their fractal dimensions were both based on very high values (typically in the range 0.98–0.99) of the coefficient of determination r^2.

Using the box-counting procedure described above, Seuront et al. [92] identified a highly significant linear behavior in log–log plots of Eq. (1) in all the male trajectories ($n = 44$) and 91.7% of the female trajectories ($n = 66$) they investigated (see their Fig. 7) for scales ranging from 1 to 200 mm (i.e. over a scale ratio $\lambda = 200$) with coefficient of determination r^2 ranging from 0.98 and 0.99 (Fig. 3(a)). In only 6 occasions (see their Fig. 8), female trajectories showed two distinct scaling behaviors for scales bounded between 1 and 10 mm ($\lambda = 10$) and 10 and 200 mm ($\lambda = 20$), with coefficient of determination $r^2 = 0.99$ (Fig. 3(b)). Note that the above mentioned two distinct scaling behaviors are not computational artifacts due to
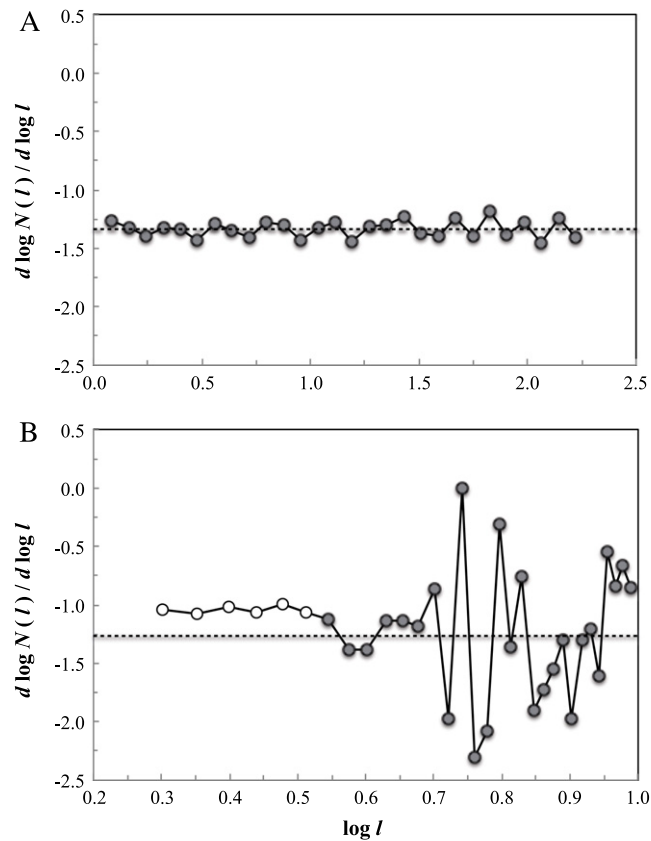
Fig. 4. Illustration of the zero-slope procedure applied to the fractal analyses previously conducted on the swimming trajectories of (A) the copepod *O. venusta* (Seuront et al. [92]; their Fig. 7 and (B) larvae of the European whitefish *C. lavaretus* (Mahjoub et al. [99]; their Fig. 4(b)). The dashed line (A) indicates the range of scales over which the slope d log $N(l)$/d log l of vs. does not significantly diverge from 0; note that the intercept ($D_b = 1.33$) returns the fractal dimension ($D_b = 1.32$) obtained by Seuront et al. [92] using the R^2-*SSR* procedure. The dotted line (B) shows the expected behavior of d log $N(l)$/d log l vs. from the fractal dimension $D_b = 1.25$ claimed by Mahjoub et al. [99]; the open dots (B) indicate the range of scales that satisfies the zero-slope procedure, and returns a fractal dimension $D_b = 1$.

box sizes being either too small compared to the resolution of the object considered – the log–log plot of $N(l)$ vs. l will artificially become flatter when the box size decreases – or too large for the size of the object, in which case the slope of log $N(l)$ vs. log l would increase when the box size increases; the exact opposite is seen in Fig. 3(b). Besides, both the scaling nature of Eq. (1) and the pertinence of the related regression analyses conducted either over scale ratios ranging from 10 to 200 are confirmed by the random pattern of the regression residuals around zero (Fig. 3(d), (e)).

Mahjoub et al. [99] also claimed they verified Eq. (1) over a scale ratio $\lambda = 5$ for the trajectories of wild and reared larvae of the European whitefish *C. lavaretus* that led to both unsuccessful and successful prey capture; see their Fig. 4 [99], and Fig. 3(c) here. However, it is readily seen from Fig. 3(c) that despite the high values of the coefficient of determination ($r^2 = 0.99$) there is a dispersion around the regression line that is not perceptible in Fig. 3(a), (b). This observation is confirmed by the convex pattern of the regression residuals around zero (Fig. 3(f)). This suggests a piecewise linear behavior, hence a continuous change of fractal dimension with scales. This behavior has serious implications: (i) it prevents the use of fractal dimension to estimate the degree of convolution of a trajectory as its absolute prerequisite – the presence of a scaling behavior – is not fulfilled [84], and (ii) it may be the signature of a Correlated Random Walk instead of actual fractality as previously demonstrated [80,81] and further discussed below.

4.2.2. Towards an objective definition of scaling ranges

A note on scale-dependent vs. scale-independent fractal dimensions. A relatively large body of literature has been devoted to assess the potential relationship between fractal dimensions and scales [140–144]. These applications of fractal analysis do not infer if (nor assume that) movement trajectories are fractal. Instead, they make use of fractal analysis to separate the range of scales into separate domains, by noting discontinuities in a plot of D vs. scale, i.e. a 'fractogram' *sensu* [140]. Practically, fractograms are obtained by using a specific range of scales, and then sliding this range along the scale axis. In this particular context, fractal dimensions D are implicitly considered scale-specific, and used to detect transitions and domains. A discontinuity in D vs. scale indicates a *qualitative* change in trajectory structure from one domain to another, i.e. a 'mixed fractal' *sensu* [145], while within domains any change in D would be continuous [144]. This approach fundamentally differs

Table 3
Review of zooplankton behavioral studies based on the scaling properties of probability distribution functions (PDFs) and cumulative density functions (CDFs) of various behavioral states.

Copepod species	Sex	Treatment	Method	PDF vs. CDF	Behavioral state				Source
					Break	Sink	Swim[a]	Jump	
C. darwini	na	na	$p(t) \approx t^{-c}$	PDF	3	–	2.8	–	[108]
C. hamatus	Female	Control ($T = 18$ °C; $S = 34$)	$P(t \leq T) \approx t^{-\phi\,\mathrm{b}}$	CDF			1.47–1.51		[70]
		Naphthalene (50–1000 µg/l)			–	–	0.71–1.29	–	
P. annandalei	Males	28 °C; $S = 15$	$p(t) \approx t^{-c}$	PDF	0.76	1.58	1.75	0.67	[109]
	Non-ovigerous females				1.85	1.84	2.12	3.03	
	Ovigerous females				1.26	2.23	1.98	2.45	
E. affinis	Males	18–19 °C; $S = 0.5$–30	$p(v) \approx v^{-c}$	PDF	–	–	2.7–3.5	–	[110]
	Non-ovigerous females				–	–	2.7–3.1	–	
	Ovigerous females				–	–	2.7–3.3	–	
	Males		$p(t) \approx t^{-c}$	PDF	2.0–2.3	–	2.8–3.2	–	
	Non-ovigerous females				2.1–2.3	–	3.1–4.3	–	
	Ovigerous females				2.1–2.3	–	2.8–3.8	–	
E. affinis	Males	Control (17–18 °C; $S = 15$)	$p(t) \approx t^{-c}$	PDF	3.5	–	–	–	[96]
		Nonylphenol (2 µg/l)			6.2	–	–	–	
	Females	Control (17–18 °C; $S = 15$)	$p(t) \approx t^{-c}$	PDF	2.4	–	–	–	
		Nonylphenol (2 µg/l)			2.9	–	–	–	
P. annandalei	Males	2D	$p(t) \approx t^{-c}$	PDF	2.8–3.7	2.7–2.9	2.0–2.8	–	[112]
		3D			4.3	3.1	2.6	–	
E. affinis	Males	Density (40–160 ind l^{-1})	$p(t) \approx t^{-c}$	PDF	2.0–2.6	3.1–3.6	3.7–4.1	–	[112]
		Tank volume (0.125–3.375 l)			2.1–2.6	3.1–4.2	3.7–4.1	–	
A. clausi	Females	Control ($T = 18$ °C; $S = 32$)	$N(l \leq L) \approx l^{-\phi}$	CDF	–	–	1.82–1.84	–	[72]
		Light[c]			–	–	1.42–1.45	–	
C. typicus		Control			–	–	1.70–1.72	–	
		Light			–	–	1.31–1.34	–	
P. parvus		Control			–	–	1.73–1.75	–	
		Light			–	–	1.46–1.48	–	
P. elongatus		Control			–	–	1.60–1.61	–	
		Light			–	–	1.42–1.44	–	
T. longicornis		Control			–	–	1.68–1.69	–	
		Light			–	–	1.20–1.23	–	
E. affinis	Males	Control ($T = 15$ °C; $S = 4$)	$N(l \leq L) \approx l^{-\phi}$	CDF	–	–	1.75	–	[73]
		PAH[d]			–	–	1.32–1.68	–	
	Non-ovigerous females	Control			–	–	1.70	–	
		PAH[d]			–	–	1.24–1.55	–	

					Static[e]	Crawl[e]	Cruise[e]	Sink[e]	
L. branchialis	Adult females[f]	Control (seawater at 10 ± 0.05 °C)	$p(v) \approx v^{-c}$	PDF	1.36	2.08	0.98	1.33	[106]
		Control$_1$[g]			1.14	2.06	1.45	1.27	
		Control			1.00	1.6	1.78	1.4	
		CCW[h]			1.29	1.54	1.29	1.35	
		Control			1.52	1.5	1.34	1.31	
		FCW[i]			1.32	1.47	1.68	1.21	
		Control			1.13	1.19	1.36	1.25	
		TCW[j]			1.31	1.31	1.62	1.23	
		Control			0.99	2.08	0.20	1.25	
		WCW[k]			1.17	1.76	0.94	1.14	

[a] Referred to as '*cruising*' in Ref. [110].

[b] The exponent ϕ (Eqs. (10) and (11)) can be directly compared to the PDF exponent c (Eqs. (8) and (9)) as $c = 1 + \phi$ [122].

[c] The stress induced by light was either related to behavioral observations conducted in the dark during the day, or under simulated daylight conditions during the night.

[d] PAH: the water soluble fraction of Polycyclic Aromatic hydrocarbons, considered at 0.01%, 0.1% and 1%.

[e] These behavioral states were defined based on both the swimming velocity (v) and the vertical position of a copepod within the experimental chamber as '*static*' and '*crawl*' when motion is restricted to the bottom respectively with $v < 3$ mm s^{-1} and $v > 3$ mm s^{-1}, and '*cruise*' and '*jump*' when motion occurs away from the bottom respectively with $3 < v < 20$ mm s^{-1} and $v > 20$ mm s^{-1}.

[f] Pre-metamorphosed adult females, free-swimming stage.

[g] Control water introduced in the experimental chamber as a control treatment.

[h] CCW: cod-conditioned water.

[i] FCW: flounder-conditioned water.

[j] TCW: trout-conditioned seawater.

[k] WCW: whiting-conditioned water.

from other applications of fractal analysis to biology and ecology that aim at identifying scaling ranges, i.e. ranges of scales where fractal dimensions are invariant, hence indicative of fractality [6,84].

In this context, I hereafter briefly rehearse two simple methods that were initially developed to infer the fractal nature of a movement trajectory by selecting objectively the appropriate range of scales to include in a regression analysis leading that estimates a fractal dimension as e.g. in Eq. (1) [91]. Notice that they can also be used to detect discontinuities in fractal dimension estimates, and lead to the aforementioned fractograms; see Ref. [6] for further details. These methods have found applications in various areas of behavioral ecology, including zooplankton (Tables 1 and 2) and birds [146]. Note, however, that what follows is a suggested methodology to infer the presence *and* the extent of a scaling range, and is by no means a criticism of the central point of previously published papers that did not use it (Tables 1 and 2).

A methodology for the identification of scaling ranges. The R^2-SSR procedure is based on a regression window of varying width ranging from a minimum of n data points to the entire data set. Note that in the original publication introducing the R^2-SSR procedure, Seuront et al. [91] erroneously states that $n = 5$ was "*the least number of data points to ensure the statistical relevance of a regression analysis*" as *stricto sensu* the minimum number of data points needed to fulfill the standardized t statistics used to infer the significativity of Pearson's correlation coefficient R is $n = 3$. However, as previously stressed elsewhere [6,84], the choice of the minimum size of a regression window is fundamentally driven by the system under study, which defines both the range of scales over which an investigator may expect to find a scaling range and the maximum number of data points available in the regression analysis. These windows are slid along the entire data set at the smallest available increments, with the whole procedure iterated $(n - 4)$ times, where n is the total number of available data points. Within each window and for each width, we estimated the coefficient of determination (r^2) and the sum of the squared residuals for the regression. The values of l (Eq. (1)), which maximized the coefficient of determination and minimized the total sum of the squared residuals, are then used to define the scaling range and to estimate the related fractal properties (Tables 1 and 2). The zero-slope procedure originates from the equivalence between Eq. (1) and $\frac{d \log N(l)}{d \log l} = -D_b$. This fact implies that (i) a scaling regime will manifest itself as a plateau in plots of $\frac{d \log N(l)}{d \log l}$ vs. log l, and (ii) the intercept of the range of scales exhibiting a zero-slope behavior provides the fractal dimension. The range of scales exhibiting a zero-slope can hence be objectively estimated using the moving regression window described above in the R^2-SSR procedure, and for each window the significance of the differences between the slope of each regression and the expected slope of 0 directly tested using standard statistical analysis, such as the modified t-test; see e.g. Ref. [147].

An illustration of identification (and misidentification) of scaling ranges. The application of the zero-slope procedure to the log–log plots of Eq. (1) observed for *O. venusta* (Fig. 3(a), (b)) and *C. lavaretus* (Fig. 3(c)) confirms the fractal nature of *O. venusta* swimming trajectories (Fig. 4(a)), but questions both the claimed fractal signature in *C. lavaretus* swimming behavior and the value of the related fractal dimension (Fig. 4(b)). Specifically, the zero-slope criterion is statistically $(P > 0.05)$ verified over the whole range of scales considered in the original analysis of *O. venusta* behavior (Fig. 4(a)), indicating that the fractal dimension is indeed scale-independent for scales ranging from 1 to 200 mm. Note that the fractal dimension returned by the intercept, $D_b = 1.33$, is statistically undistinguishable $(P > 0.05)$ from the dimension reported in Seuront et al. [92], i.e. $D_b = 1.32$. In contrast, the fractal dimension of the swimming trajectories of *C. lavaretus* drastically changes with scales (Fig. 4(b)). The zero-slope criterion is hence only verified for a very limited range of scales (Fig. 4(b)), which leads to $D_b = 1$ (Fig. 4(b)). This clearly differs from both the scaling regime claimed over the whole range of available scales, and the related fractal dimension $(D_b = 1.25)$ reported by Mahjoub et al. [99]. A close examination of the other log–log plots of log $N(l)$ vs. using the zero-slope procedure provided by Mahjoub et al. [99], see their Fig. 4, also shows that their fractal dimensions change with scales, hence genuinely questions the claimed fractality of *C. lavaretus* swimming trajectories.

There is still room for improvement to ensure the pertinence of future fractal analysis of zooplankton swimming behavior as nearly 50% of the 44 fractal studies examined here (Tables 1 and 2) do not mention explicitly the use of any criteria of fitting quality, 23% used linear regression and the coefficient of determination r^2, and only 28% used one (or both) of the objective optimization procedures detailed above. Notice that none of these studies explored the potential scale-dependence of the fractal dimensions estimated from zooplankton swimming trajectories, in contrast to other areas of behavioral ecology such as ornithology [142] or mammology [141,143,144].

There also still seems to be a misconception about the use of fractal analysis in zooplankton ecology, as I regularly witnessed students and colleagues mentioning fractal dimensions as a way to "*estimate the degree of convolution of a trajectory, not at demonstrating the fractal nature of copepod behavior*". However, as stated above and elsewhere (see e.g. Refs. [80,81]), a fractal dimension is meaningful *only if* scaling properties are unambiguously demonstrated over a significant range of scales [84], hence if the underlying behavior is fractal. Note that this misconception does not seem to appear in other areas such as the behavioral ecology of intertidal gastropods [19,148] where fractal dimensions are non-ambiguously defined as "*a scale-independent geometrical description of the shape of the spatial movement patterns*" [19].

4.3. Fractal walks vs. correlated random walks

The aforementioned lack (or limited) use of objective criteria to chose the range of scales used to estimate fractal dimensions is also at the core of what Turchin [80] coined as "*the fractal dimension is not constant but changes continuously with scales*" in reference to the piecewise linear signature returned by a Correlated Random Walk in log–log plots of Eq. (1). Note that as a consequence, if an organism moves according to a Correlated Random Walk, fractal analysis of that movement

is not justified [80,81,149]. Correlated Random Walks are intrinsically non-fractal models, hence cannot be characterized using fractal dimensions.

Correlated Random Walks may, however, *erroneously* return a fractal signature especially when the range of scales available in the analysis (i.e. the number of data points) is limited [80,81,149]. This can also be the case as log–log plots of $N(l)$ vs. l by the fractal analysis of a Correlated Random Walk as these plots can appear relatively, even very, linear depending on the parameters used to simulate the Correlated Random Walk; see Ref. [149] for a detailed discussion on the topic. In zooplankton ecology, a few simulation studies [94,97,100] analyzed the properties of simulated Correlated Random Walks using a three-dimensional box-counting method. They found that "*the regression lines of the log–log plots fit the points with good accuracy*" ($r^2 \approx 0.99$), and the resulting fractal dimensions were used to assess the "*morphological complexity of the trajectories*". Note that the issue related to the analysis of Correlated Random Walks with fractal methods is not limited to zooplankton behavioral ecology as e.g. a recent study of manta rays foraging behavior characterized tracks that are both non-significantly and significantly different from a Correlated Random Walk using fractal dimensions [150].

To my knowledge no attempt has been made to infer the presence of Correlated Random Walk in plankton behavior. To avoid erroneously considering a Correlated Random Walk as returning a fractal signature, prior to fractal analysis, it should hence be tested, as a null hypothesis, whether a Correlated Random Walk model adequately describes the properties of the swimming trajectories. I hence briefly describe hereafter a simple procedure to determine whether a zooplankton organism moves according to a Correlated Random Walk model, using the CRW_{Diff} statistic [143,144]:

$$CRW_{Diff} = \frac{1}{k} \sum_{n=1}^{k} \left(\bar{R}_n^2 - E(R_n^2) \right) / (n\bar{l})^2 E(R_n^2) \qquad (2)$$

where $\bar{R}_n^2$ is the observed mean net distance squared for each of n consecutive moves, $\bar{l}$ is the mean move length and $E(R_n^2)$ is the expected square of the net distance traveled if the organism moves following a CRW given by [151]:

$$E\left(R_n^2\right) = nE(l^2) + 2E(l)^2 \frac{c}{1-c} \left(n - (1 - c^n)/(1 - c) \right) \qquad (3)$$

where c is the mean cosine of the turning angle θ, and l is the length of one move. Under the null hypothesis of a CRW, CRW_{Diff} has a zero mean. Positive CRW_{Diff} values indicate directed walks (with a maximum value at 1), while negative values indicate trajectories that cover a shorter distance than a CRW. Confidence intervals of CRW_{Diff} are calculated by treating the squared net distance traveled for each segment of n moves as independent samples [143]. If the null hypothesis is to be rejected, it is still necessary to assess objectively the nature of the signature of the log–log plot of $N(l)$ vs. l to ensure the reality of a fractal signature.

4.4. On the actual fractality of fractal signatures

The fractal signature of Correlated Random Walks (or more generally the fractal signature of any non-fractal pattern or process) can essentially be erroneously considered as the expression of a fractal behavior when the scaling range is narrow, i.e. typically smaller than 1 decade – a recurring issue in ecological studies [6,84] – and leads to what is called *apparent fractality* [79]; see also Refs. [82,83] for a review and a discussion of the issue of narrow scaling ranges in physical systems. As a consequence, the relevance of any fractal analysis (hence the reliability of fractal dimension estimates) increases with the range of scales exhibiting a fractal signature [79,82,83], hence unambiguous information about the range of scales used to fit Eq. (1) are needed. This is potentially a critical issue in zooplankton behavioral ecology as the scaling regime has explicitly been provided in only 14% of the 44 published fractal-related studies examined here, and the extent of the scaling regime was available indirectly through a careful examination of their log–log plots in 32% of them (Tables 1 and 2).

For instance, in a study of the swimming behavior of the calanoid copepod *P. annandalei* [77], despite methodological statements related to the minimum box size "*set to* 1 mm" and that "*trajectories shorter than* 1 cm *were rejected to ensure a minimal degree of space occupation*", no information related to the range of scales over which Eq. (1) was fitted were provided. Similar conclusions and criticisms can be drawn from a study of the behavior of the parasitic copepod *Lernaeocera branchialis* [106]. These authors ran their fractal analysis for scales ranging from the size of an adult female (1.6 mm) to the closest 2^n (i.e. $2^6 = 64$) value approximating the width of their experimental arena (75 mm), and claimed that "*this range was selected to ensure that an appropriate range of scales was covered to reliably estimate F* (i.e. the fractal dimension D_b; see Eq. (1)) (Turchin, 1996; Halley et al., 2004)". They did not, however, provide either a quantitative assessment of the goodness-of-fit of Eq. (1) or the actual range of scales used to fit Eq. (1). In any case, the best possible scaling range achievable with their experimental design ($\lambda = 40$) is still relatively narrow *sensu* [80,84], who by no means supported the idea that a scaling range of 40 ensures, that "*an appropriate range of scales was covered to reliably estimate the fractal dimension*" as claimed by Brooker et al. [106]. As discussed in the present work (see text above, and Figs. 3 and 4) and elsewhere [6], the range of scales available to fractal analysis and the range of scales exhibiting a power-law relationship are two distinct issues, even if the relevance and reliability of fractal analysis increases with the range of scales exhibiting a fractal signature [79,82,83].

Finally, note that even when the scaling range is (directly or indirectly) provided, it is generally relatively narrow, typically in the range 0.5–2 decades (see Tables 1 and 2). This is consistent with the values reported for the fractal structures identified in a vast range of physical systems [79,82,83] and ecological systems [6,84]. The collection of data over a wider range of

scales is one avenue to test the true value of fractals methods in ecology to avoid the fashionable tendency to see '*fractals everywhere*' stressed by Halley et al. [84]. This is not easily achievable, however, as there is a limit to how much the range of scales available in the analysis can be increased, as every order of magnitude scale increase requires a non-trivial 10- to 1000-fold increase in the data array. In zooplankton behavioral ecology, the range of scales available is implicitly bounded by the size of the organism and the experimental container and by the limits of optical systems, which urges the need to use objectives fitting procedures to optimize the relevance of fractal analysis.

4.5. Do size, shape and position matter?

I now briefly describe how the length, orientation and placement of an object with respect to the initial box used to implement Eq. (1) are all potential causes of errors linked to the intrinsically discrete nature of the box-counting algorithm that can propagate into significant biases in the estimates of fractal dimension. This limitation can be illustrated *a minima* with the simple example of a line segment embedded in a two- or three-dimensional space. Let us start with the fact that the box-counting algorithm will return the value $D_b = 1$ for a line segment *only if* (i) the box side and the line have an equal length (or the line length is a linear function of the scale ratio between two steps of the box-counting algorithm implementation), and (ii) the line is either vertical or horizontal. If the former condition is not fulfilled, the box-counting algorithm may lead to artificially increase the number of empty boxes, hence to decrease the fractal dimensions. In contrast, if the latter condition is not fulfilled, different values of the angle between the line segment and the side of the box may lead to either increase or decrease the number of empty boxes, hence respectively increase or decrease the fractal dimensions; see e.g. Ref. [152] for a discussion. These two sources of error can be readily fixed by ensuring that the bounding box side coincides with the width of the segment line, and the larger box must be framed so that the segment line is parallel and touches the edges. The situation may become drastically more difficult to handle when far more complex shapes such as zooplankton trajectories are considered.

A procedure leading to minimize the aforementioned sources of error is described hereafter. It shares the idea of box size ranging for each trajectory from the size of the organism under interest and its maximal three-dimensional displacement with other studies [77,104]. This method differs, however, as it uses systematic replicates of grid orientation in the box-counting algorithm. This approach specifically minimizes the potential biases related to both the anisotropy of the swimming trajectory and the initial position of the overlying three-dimensional grid of orthogonal boxes [6,91]. For each box size l, the grid is incrementally rotated of an angle α, where α ranges from 0 to $\pi/4$ in the x–y plane, and from 0 to $\pi/4$ in the x–z plane. The resulting distributions of fractal dimensions, estimated from each combination of the angles α_{x-y} and α_{x-z}, are averaged, and the resulting dimension used to characterize the complexity of a swimming trajectory. The method is validated if none of the returned fractal dimensions were statistically significantly different from (i) dimensions $D = 1$ and $D = 2$ when respectively run on vectors of random length and orientation and on surfaces of random surface and orientation, and (ii) the expected fractal dimensions of theoretical fractal objects such as the well-known Koch snowflake ($D = 1.262$), the Koch island ($D = 1.5$), the Sierpinski carpet ($D = 1.893$) and the Sierpinski gasket ($D = 1.585$) [105]. Michalec et al. [77,104] followed a slightly different approach through a script calibrated with vectors of random length and orientation in the three-dimensional space through a principal component analysis. Principal component analysis was used to minimize the perpendicular distances from the data to the fitted model and proposed as an appropriate method to fit a linear regression to scattered 3D data. The discrepancy between the observed fractal dimension of the straight line ($D = 1.033$ in Ref. [77]) and its expected value ($D = 1$) was used as a correction factor in the computation of the fractal dimension of the trajectory. Note, however, that their algorithm returned fractal dimension below the lower limit $D = 1$; see their Fig. 8 [77]. Wasserman and Vink [78] first estimated the fractal dimension of a straight line ($D = 0.97$) and subsequently used the deviation to its expected dimension ($D = 1$) as a correction for fractal dimension estimated from swimming trajectories.

4.6. 2D vs. 3D fractality, the question of isotropy

The aforementioned procedures will return an integrated, spatially-averaged, fractal dimension. In case of an anisotropic swimming trajectory, this approach may, however, implicitly hide potentially relevant information such as discrepancies in the degree of space-filling of the trajectory in the horizontal and vertical dimensions of the three-dimensional domain. This has been illustrated in detail by the fractal dimensions of the swimming trajectories of the cladoceran *Daphnia pulex* [91] that were consistently significantly lower in the horizontal plane ($D_{x-y} = 1.11 \pm 0.06$) than in the vertical planes x–z ($D_{x-z} = 1.21 \pm 0.05$) and y–z ($D_{y-z} = 1.20 \pm 0.07$). The complexity of the vertical components of the *D. pulex* swimming trajectories is then higher than the one of its horizontal components, suggesting that the vertical swimming behavior of *D. pulex* is more complex than the horizontal ones. Note that the average of D_{2xy}, D_{2xz} and D_{2yz} is not significantly different from the three-dimensional fractal dimension of the trajectories D_3 ($D_3 = 1.18 \pm 0.06$), due to the intrinsic three-dimensional integrative properties of Eq. (1). Note, that a three-dimensional fractal dimension implicitly may, however, carry less information than the fractal dimensions of their two-dimensional projections. A meaningful three-dimensional fractal analysis hence requires a critical assessment of its potential fractal anisotropy; for instance this approach led Mahjoub et al. [103] to identify an isotropy and an anisotropy in the swimming behavior of Malabar grouper (*Epinephelus malabaricus*) larvae in the presence and absence of prey, respectively. In their study of the swimming behavior of *P. annandalei* Michalec et al. [77] examined

the magnitude of the horizontal and vertical components of the velocity vectors, and found that the horizontal component was on average 1.5 times larger than the vertical one for all three adult stages. While this indicates a form of anisotropy in *P. annandalei* swimming behavior, no mention was made about the potential anisotropy in their fractal dimension.

As a conclusion, it is recommended to consider explicitly the fundamentally three-dimensional nature of zooplankton swimming behavior (i) to accurately estimate critical parameters such as swimming speed and the time spent in various behavioral states [112], to avoid the confusion between swimming downward and sinking [73,105,112] and (ii) to objectively infer the isotropic character of a given species motion [6,91,103].

4.7. Which fractal dimension is my fractal dimension?

A vast majority (ca. 80%) of the papers analyzed here did not estimate the fractal dimensions of the observed swimming trajectories with more than one technique (Table 1). In addition, most of them did not compare their estimates to any of the fractal dimensions reported in the literature for ichthyoplankton and zooplankton swimming trajectories that typically fall in the range 1.0–1.8 [69,71–73,77,89,91–95,97,98,101,102,104–106,119]. Practical approaches to measure fractal dimensions have, however, not yet been standardized and not all fractal dimension are comparable; see Ref. [6] for a review of fractal methods and comparison of their fractal dimensions. As such, the reliability of fractal dimension estimates can also be increased through the application of different methods on a given swimming trajectory. In addition to the box-counting method, two conceptually similar methods described below are very well adapted to the characterization of swimming trajectories, the divider dimension method and the mass dimension method.

The divider dimension D_d (also referred to as the compass dimension; [91]) was estimated – in 7 of the 24 papers (29.2%) reviewed in Table 1 – by measuring the length of a trajectory at various scales δ. The procedure is analogous to moving a set of dividers (like a drawing compass) of fixed length δ along the trajectory. The estimated length of a trajectory $L(\delta)$ increases with increasing δ as:

$$L(\delta) \propto \delta^{1-D_d}. \tag{4}$$

Noticing that the estimated length $L(\delta)$ is the product of $N(\delta)$ (the number of compass dividers required to cover the trajectory) and δ ($L(\delta) = N(\delta)\delta$), Eq. (4) can be written as:

$$N(\delta) \propto \delta^{-D_d}. \tag{5}$$

Note that Dowling et al. [89] incorrectly quoted Eq. (4) as $L(\delta) \propto \delta^{-D_d}$; this error cannot, however, explain their fractal dimensions $D_d < 1$.

The mass dimension method, used in only 2 of the 24 papers reviewed in Table 1, counts the number of pixels occupied by a trajectory in cubic ($\delta \times \delta$) sampling windows. The mass $m(\delta)$ of occupied pixels is subsequently defined as $m(\delta) = N_O(\delta)/N_T(\delta)$, where $N_O(\delta)$ and $N_T(\delta)$ are respectively the number of occupied pixels and the total number of pixels within an observation window of size δ. These computations are repeated for various values of δ, and the mass dimension D_m is defined as:

$$m(\delta) \propto \delta^{D_m} \tag{6}$$

where the fractal dimension D_m is estimated from the slope of the linear trend of the log–log plot of $m(\delta)$ vs. δ.

It is readily seen from Eqs. (1) and (5) that $D_b = D_d$, while more convoluted developments show that $D_b = D_m$, hence $D_b = D_d = D_m$; see Ref. [6] for details. Statistically inferring the absence of significant differences between fractal dimensions returned by different methods of analysis hence constitutes an additional guarantee of the trustworthiness of the fractal dimension estimates.

5. From self-similar to self-affine fractals

5.1. Definition

As described above, fractals are scale-independent geometric objects. However, scale-independence can be dichotomized into *self-similar* and *self-affine* fractals. An object is called self-similar if it may be written as a union of rescaled copies of itself, under the condition of an isotropic (i.e. uniform in all directions) rescaling. For instance, theoretical fractal objects such as the Cantor set (Fig. 5(a)) display exact self-similarity; in other words there are no upper and lower bounds to their fractality, i.e. Eqs. (1), (4) and (6) will display linear log–log plots whatever the spatial scales considered may be. Unlike theoretical fractals, natural fractal objects do not display exact self-similarity. Instead they display self-similarity at least over a limited range of scales, corresponding to partial self-similarity; Eqs. (1), (5) and (6) will hence exhibit a power-law only over a limited range of scales (Fig. 3(b)). For example, lung branching shows self-similarity over 14 dichotomies, and tree branching over 8 dichotomies. Note, however, that in zooplankton behavioral ecology, partial self-similarity is essentially controlled by experimental constraints. For instance, in zooplankton studies the lower and upper spatial and temporal scales accessible for behavioral analysis are intrinsically limited by the temporal resolution of the camera, the time needed by an
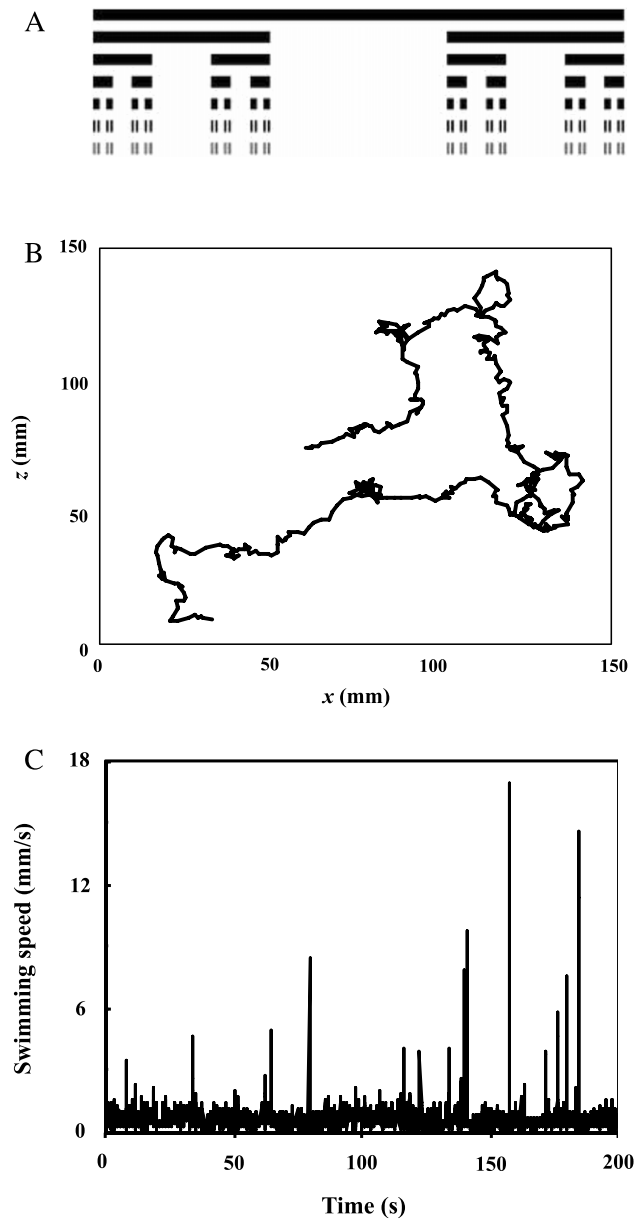
Fig. 5. Illustration of the fundamental differences between exact (A) and statistical (B) self-similar fractal objects, and self-affine fractal objects (C). The theoretical Cantor set (A) displays exact self-similarity, as it is constructed following the same rule at each step of the construction, that is a given line segment is divided into thirds, the central part is removed, the procedure is repeated on the two remaining third, and after an infinite number of iterations, this converges to a set of points or Cantor set, also referred to as Cantor dusts. The fractal dimension of the Cantor set is dependent on the scale ratio applied between two successive steps, here at each step there are two elements that are three times smaller than the original one, hence $D = \log 2 / \log 3 = 0.631$. A copepod trajectory (B) displays partial self-similarity (here a two dimensional projection of the 3D trajectory of an adult male *E. affinis*; see Seuront [105], his Fig. 2(a)). In contrast, the time series of the instantaneous velocities of an adult male *E. affinis* (C) along his trajectory is self-affine in a sense that the *x*-axis and the *y*-axis correspond to distinct physical quantities, i.e. time and velocity.

organism to reach the wall of the container, the size of the organisms under consideration and the size of the experimental containers.

In contrast, an object is called *self-affine* if it may be written as a union of rescaled copies of itself, where the rescaling is anisotropic (i.e. dependent on the direction). Consider, for example, the velocity of the copepod *Eurytemora affinis* measured as a function of time (Fig. 5(c)) along the trajectory shown in Fig. 5(b). It looks rough, like the boundary of a random fractal, with the two axes corresponding to physical quantities (velocity and time) that are intrinsically different. In general, whenever different quantities involved in such constructions scale differently, the notion of self-similarity contained in Eqs. (1), (4) and (6) will not be adequate; to describe these phenomena, one needs the more versatile machinery of self-affinity.

5.2. Dimension of self-affine fractals

5.2.1. Spectral analysis

Spectral analysis is an expression of the variance (*stricto sensu* the square of the amplitude of the Fourier transform) of a descriptor at different temporal or spatial scales. In practice, the power spectral density $E(x)$ is given by

$$E(x) \propto x^{-\beta} \tag{7}$$

where x is the frequency (s^{-1}; $f = 1/t$, where t is time) or the wavenumber k (m^{-1}; $k = 1/l$, where l is space) for temporal and spatial self-affine processes, respectively. The spectral exponent is estimated as the slope of a log–log plot of Eq. (7) using one of the fitting procedures described above.

Brownian motion (i.e. normal diffusion) is characterized by $\beta = 2$. Anti-persistent and persistent fractional Brownian motions (fBm) are characterized by $\beta < 2$ and $\beta > 2$, respectively. In contrast, anti-persistent and persistent fractional Gaussian noises (fGn) are respectively characterized by $\beta < 0$ and $\beta > 0$. Note that fractional Gaussian noises and fractional Brownian motions differ in that they are respectively stationary and non-stationary processes. Briefly put, stationary processes fluctuate by a relatively constant degree around a mean value that remains relatively constant over time (Fig. 6(a)–(c)), whereas for a non-stationary process the statistical moments of the process (e.g. mean and variance) are time-dependent (Fig. 6(d)–(e)). More specifically, a fractional Gaussian noise is defined as the successive increments of a fractional Brownian motion, and a fractional Brownian motion is the result of the cumulative sum of a fractional Gaussian noise; see Ref. [153] for a detailed description of the dichotomy between fractional Gaussian noises and fractional Brownian motions. In terms of motion behavior, *anti-persistence* means that increases in the signal (for fGn) or in the increments of the signal (for fBm) are more likely to be followed by decreases, and *vice versa* decreases are more likely to be followed by increases; Fig. 6(a), (d). In contrast, *persistence* implies that increases in the signal (for fGn) or in the increments of the signal (for fBm) are more likely to be followed by further increases, and decreases are likely to be followed by decreases (Fig. 6(c), (f)). Anti-persistent and persistent processes contain structure that distinguishes them from truly random sequences of data. The spectral exponent β can subsequently be expressed as a fractal dimension, the Fourier dimension D_{FFT} as Ref. [46] $D_{FFT} = D_E + 1 - (\beta - 1)/2$ for fractional Brownian motions, and $D_{FFT} = D_E + 1 - (\beta + 1)/2$ for fractional Gaussian noises, where D_E is the Euclidean dimension of the embedding space, e.g. $D_E = 1$ for a time series of successive displacements (see Fig. 5(c)).

Spectral analysis has still barely been used in zooplankton behavior (Table 2), and returned a relatively wide range of values of the spectral exponent β depending on the species considered. For instance, the velocity components of *D. pulex* and *Clausocalanus furcatus* were both characterized by $\beta \approx 0$ [98,107], indicative of a random process without internal serial correlation. In contrast, β ranged from 0.3 to 0.75 in *Temora longicornis* [116], and 1.4 to 1.5 in *P. annandalei* [109]. This suggests that zooplankton organisms exhibit a range of behavior including fractional Gaussian motion, fractional Gaussian noise and pure random noise.

5.2.2. Probability density functions

Self-affine techniques based on the analysis of frequency distributions have also been used in zooplankton behavioral studies (Table 2). They include consideration of the scaling properties of the probability distribution functions (PDFs) of either the time t_x spent in a specific behavioral state x [108–110,112]:

$$p(t_x) \propto t_x^{-c} \tag{8}$$

or the velocity v_x used to defined different behavioral states x:

$$p(v_x) \propto v_x^{-c}. \tag{9}$$

Various behavioral states have been considered through Eqs. (8) and (9) in the literature (Table 3). They include (i) break (no motion) and slow swimming in *Cosmocalanus darwinii* [108], (ii) break, sinking, cruising and fast swimming in *E. affinis* [110], (iii) break, swim, jump and sink in *P. annandalei* [109], (iv) break, cruise and sink in both *E. affinis* and *P. annandalei* [112], (v) static, crawling, cruising, fast swimming and sinking in *L. branchialis* [106], and (vi) generic instantaneous speed in *E. affinis* [114] (Tables 2 and 3).

The values of the exponent c returned by Eqs. (8) and (9) for a range of species under various experimental conditions are reported in Table 3. Note, however, that some of the values reported in Table 3 should be considered with an extreme caution. Indeed, none of the above-mentioned studies used any objective optimization procedures to choose the range of t_x or v_x values over which to fit Eqs. (8) and (9), respectively. In some cases, it is also unlikely that most of the log–log plots of $p(t_x)$ vs. t_x (see Ref. [109], their Fig. 6, and [112], their Fig. 5), and $p(v)$ vs. v (where v is the swimming speed; [110], see their Fig. 2) may satisfy the scrutiny of any of the objective optimization procedures described above. In particular, the exponents c estimated for the 'jump' behavioral state in *P. annandalei* females and males are based on respectively only three and two points ([109]; see their Fig. 6(c) and their Table 3); the former is at best highly questionable, while the latter is fundamentally fallacious as based on a mathematical heresy.

It is also stressed that the potential amalgamation between actual sinking and vertical downward swimming, as well as the author-related differences in the definition of a given behavior – see e.g. Ref. [105] for a discussion on the topic –
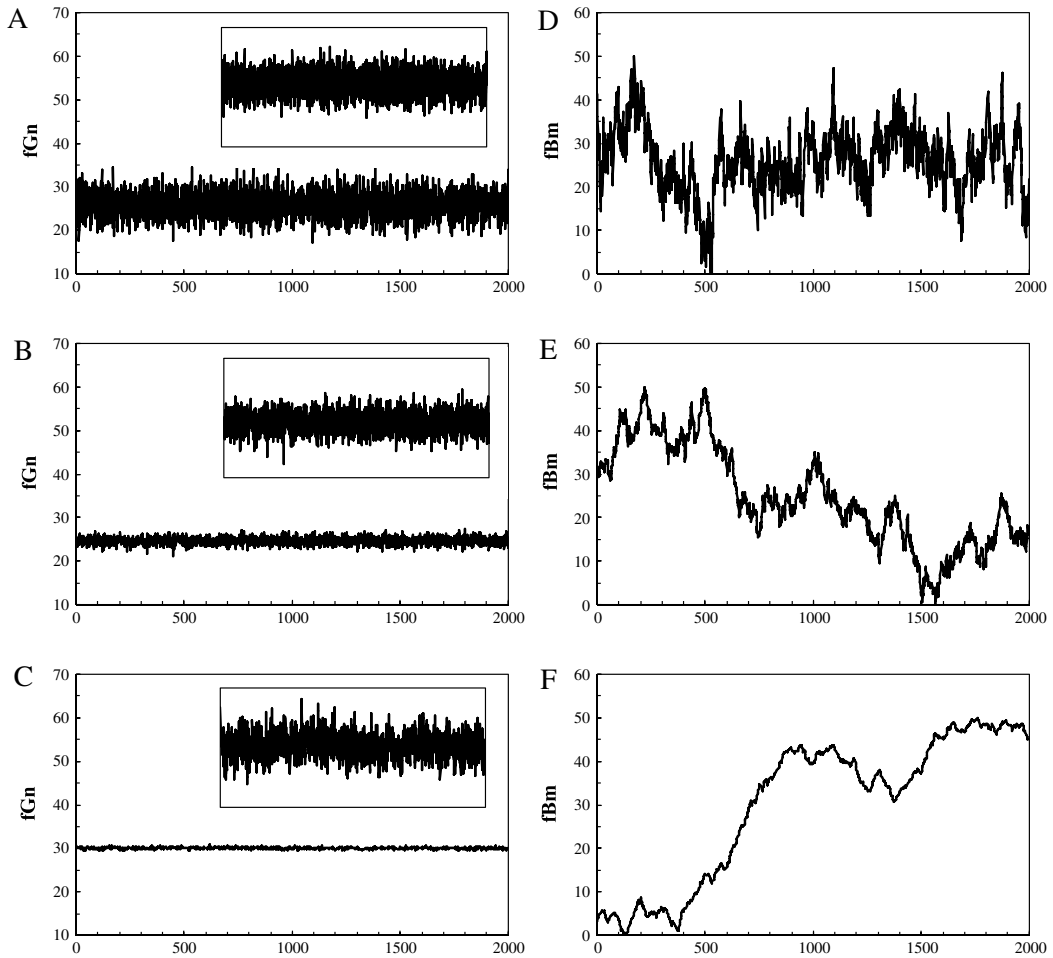
Fig. 6. Examples of fractional Gaussian noises (fGn; A–C) and fractional Brownian motions (fBm; D–F) characterized by a Hurst exponent $H = 0.25$ (A, D), $H = 0.5$ (B, E) and $H = 0.75$ (C, F). Note the one-to-one correspondence between fGn and fBm; a stationary fractional Gaussian noise constitutes the successive increments of a non-stationary fractional Brownian motion, and reciprocally a fractional Brownian motion is the result of the cumulative sum of a fractional Gaussian noise. The insets show details of the fGn.
Source: Modified from Ref. [6].

likely impacts the values of the exponent c estimated for both sinking and swimming. As such, this may – to some extent and beyond the inherent behavioral differences related to different species and experimental conditions and treatments – explain the observed variability between the exponents c (Table 3). This variability is particularly pronounced in the behavior of *L. branchialis* [106] as the relative differences between the exponents c estimated in control water and in an experiment where control water was introduced in the experimental chamber as a control treatment for the '*static*' (1.19), '*crawl*' (1.01), '*cruise*' (0.68) and '*sink*' (1.05) swimming states strongly overlap with those estimated in control water and after the introduction of water conditioned by the smell of a few fish species that are respectively in the range 0.78–1.15, 0.91–1.04, 0.21–1.38 and 1.02–1.08. While the resolution of this specific issue goes far beyond the scope of the present work, this observation may suggest that the effect of the experimental design on swimming behavior is of the same magnitude or even greater than the behavioral effect induced by most of the actual treatments.

Finally, a strong discrepancy is also noted in the use of Eqs. (8) and (9). Specifically, most (80%) of the published reports that investigated the PDFs of the time t_x spent in a specific behavioral state x actually studied the scaling properties of Eq. (8). In contrast, 80% of the published work that considered the PDFs of the velocity v_x characterizing a behavioral state x did not actually study the scaling properties of Eq. (9) (Table 2). Instead, these studies assessed eventual differences in the shape of a log–log plots of $p(v_x)$ vs. v_x. For instance, a few papers applied Eq. (9) to assess eventual differences in the shape of a log–log plot of $p(v_x)$ vs. v_x between (i) *E. affinis* males, ovigerous females and non-ovigerous females exposed to the presence of the predatory *Dicentrarchus labrax* larvae [120], (ii) *P. annandalei* males and *E. affinis* males observed in experimental containers of different volumes and under various conditions of individual concentrations [115], (iii) *T. longicornis* males and females exposed to different food treatments [116], and (iv) *P. annandalei* males, females and ovigerous females respectively exposed to various waterborne pollutants [104] and to a diatom toxin [119].

5.2.3. Cumulative probability distribution functions

A few studies have investigated the scaling properties of the cumulative probability distribution functions (CDFs) of move durations T greater than a determined duration t in the calanoid copepod *Centropages hamatus* [70]:

$$p(t \leq T) \propto t^{-\phi} \tag{10}$$

and move lengths L greater than a determined length l in a range of calanoid copepod species, i.e. *Acartia clausi, Centropages typicus, Paracalanus parvus, Pseudocalanus elongatus* and *T. longicornis* [72] and *E. affinis* [73]:

$$N(l \leq L) \propto l^{-\phi}. \tag{11}$$

The values returned by Eqs. (8)–(11) for a range of species under various experimental conditions are reported in Table 3. Note that there is a one-to-one correspondence between the exponents c and ϕ obtained *via* the scaling properties of PDFs and CDFs, i.e. $c = 1 + \phi$ [122].

6. From fractals to multifractals

6.1. A first step towards multifractals

To my knowledge, the first published work that ever used the concept of multifractals in marine biology and ecology, entitled '*Intermittency in the plankton: a multifractal analysis of zooplankton biomass variability*' [61], went well beyond the concept of fractal itself, that had still seldom been used since then; see also Seuront [6] for a more general review on the subject. Following Feder [125], a measure (i.e. a physical quantity such as mass, energy, a number of individuals, or more specifically the distance displaced by a copepod) has to be distinguished from its geometric support, which might or might not have a fractal geometry. Then, if a measure has different fractal dimensions on different parts of the support, the measure is a multifractal. Multifractals are hence a generalization of fractal geometry initially introduced to describe the relationship between a given quantity and the scale at which it is measured. While fractal geometry describes the complexity of a given pattern with the help of only one parameter (the fractal dimension), multifractals characterize its detailed variability by an eventually infinite number of sets, each with its own fractal dimensions.

6.2. A step further: multifractals as a diagnostic tool to assess a family of diffusive search patterns

Multifractals have been used to describe the intermittency (very rare and violent fluctuations interspersed between areas of relative stasis) in time series, transects or vertical profiles of ocean passive scalars temperature, salinity, turbulent shear, phytoplankton and zooplankton biomass [46–49,63,154–158]. In zooplankton behavioral ecology, multifractals quantifies the intermittent nature of the successive displacements of a range of species (Fig. 5(c), Table 4), including the cladoceran *D. pulex* [159], and the calanoid copepods *T. longicornis* [113,159,160], *P. annandalei* [109,112,115], *E. affinis* [109,112, 113,115], and *Calanus sinicus* [161]. Specifically, the strongly non-Gaussian fluctuations perceptible in copepod successive displacements that range from very likely slow steps to rare and extremely rapid displacements (Fig. 5(c)) are inherently incompatible with classical self-affine approaches based e.g. on the scaling behavior of the power spectral density (Eq. (8)) or the root-mean-square fluctuation of the displacement ($R(t) \propto t^{\alpha}$; [162]) – see Refs. [6,163] for further examples – that are limited to second-order moments. A more general approach is based on the analysis of qth order long-range correlations in copepod displacements. Specifically, the norm $\|\Delta X_{\tau}\|$ of copepod three-dimensional displacements is defined from $X_{\tau} \equiv (x_t, y_t, z_t)$ coordinates as $\|\Delta X_{\tau}\| \equiv \sqrt{(x_{t+\tau} - x_t{}^2 + (y_{t+\tau} - y_t)^2 + (z_{t+\tau} - z_t)^2)}$, where τ is the temporal increment, and (x_t, y_t, z_t) and $(x_{t+\tau}, y_{t+\tau}, z_{t+\tau})$ are respectively the positions of a copepod at time t and $t+\tau$. $\|\Delta X_{\tau}\|$ is a non-stationary process with stationary increments, its statistics do not depend on time, t, but on the temporal increment τ [6]. The moments of order q ($q > 0$) of the norm of three-dimensional displacements $\|\Delta X_{\tau}\|$ depend on the temporal increment τ as:

$$\langle \|\Delta X\|^q \rangle \propto \tau^{\zeta(q)}. \tag{12}$$

The exponents $\zeta(q)$ are estimated as the slope of the linear trend of $\langle \|\Delta X\|^q \rangle$ vs. τ in log–log plots using the objective optimization criteria defined above. The moment function $\zeta(q)$ characterizes the statistics of the random walk $\|\Delta X_{\tau}\|^q$ of the copepod regardless of the scale and intensity [6,113]. Low and high orders of moment, q, characterize respectively smaller and more frequent displacements, and larger and less-frequent displacements. Note the one-to-one correspondence between the function $\zeta(q)$ and the spectral exponent β for $q = 2$, i.e. $\beta = 1 + \zeta(2)$ [49].

The shape of the function $\zeta(q)$ can be used as a direct, objective and quantitative diagnostic tool to unambiguously identify the type of motion exhibited by copepods, and ultimately any swimming organisms (Fig. 7) [113]. Briefly, for Brownian motion, $\zeta(q) = q/2$, and fractional Brownian motion is defined as $\zeta(q) = qH$ where $H = \zeta(1)$, with the limits $\zeta(q) = 0$ and $\zeta(q) = q$ corresponding respectively to confinement and localization, and ballistic motion. Note that because a fractional Brownian motion is the fractional integration of order h of a Gaussian noise [164], the function $\zeta(q)$ can also be written as $\zeta(q) = q(h - 1/2)$; the Brownian motion case corresponds to the special case $h = 1$ (i.e. an ordinary integration of a Gaussian white noise), hence $H = 1/2$. Anomalous diffusion occurs when $H \neq 1/2$. Specifically,

Table 4
Review of zooplankton behavioral studies based on self-affine multifractal methods.

Organism	Species	Method	Scaling range	Optimization criteria	2D vs. 3D	Source
Crustacean (Copepoda)	T. longicornis	$\langle \|\Delta X_\tau\| \rangle \approx \tau^{\zeta(q)}$	100	na	3D	[160]
Crustacean (Copepoda)	T. longicornis	$\langle \|\Delta X_\tau\| \rangle \approx \tau^{\zeta(q)}$	100	R^2-SSR; zero-slope	3D	[159]
Crustacean (Cladocera)	D. pulex	$\langle \|\Delta X_\tau\| \rangle \approx \tau^{\zeta(q)}$	67	R^2-SSR; zero-slope	3D	
Crustacean (Copepoda)	P. annandalei	$\langle \|\Delta X_\tau\| \rangle \approx \tau^{\zeta(q)}$	100[a]	R^2-SSR	2D	[109]
Crustacean (Copepoda)	P. annandalei	$\langle \|\Delta X_\tau\| \rangle \approx \tau^{\zeta(q)}$	na	R^2-SSR	2D/3D	[115]
	E. affinis	$\langle \|\Delta X_\tau\| \rangle \approx \tau^{\zeta(q)}$	na	R^2-SSR	2D/3D	
Crustacean (Copepoda)	P. annandalei	$\langle \|\Delta X_\tau\| \rangle \approx \tau^{\zeta(q)}$	na	R^2-SSR	3D	[112]
Crustacean (Copepoda)	C. sinicus	$\langle \|\Delta X_\tau\| \rangle \approx \tau^{\zeta(q)}$	na	na	2D	[161]
Crustacean (Copepoda)	P. annandalei	$\langle \|\Delta X_\tau\| \rangle \approx \tau^{\zeta(q)}$	50[a]	na	3D	[119]
Crustacean (Copepoda)	T. longicornis	$\langle \|\Delta X_\tau\| \rangle \approx \tau^{\zeta(q)}$	1000	R^2-SSR	3D	[113]
Crustacean (Cladocera)	E. affinis	$\langle \|\Delta X_\tau\| \rangle \approx \tau^{\zeta(q)}$	1000	R^2-SSR	3D	

[a] The scaling ranges were not explicitly provided, but estimated graphically from the figures of the published work.

super-diffusion occurs when $H > 1/2$, and sub-diffusion when $H < 1/2$. For finite-length Lévy flights (and truncated Lévy flights [165]), the function $\zeta(q)$ is bilinear with $\zeta(q) = q/(\mu - 1)$ for $q < \mu - 1$ and $\zeta(q) = 1$ for $q \geq \mu - 1$; the exponent μ $(1 < \mu \leq 3)$ characterizes the power-law tail of the probability distribution of the move-step length l as $P(l) \approx l^{-\mu}$, where $1 < \mu \leq 3$. For $\mu \geq 3$ the mean and the variance of the move-step-lengths are both finite, hence as a consequence of the central-limit theorem, their distribution is Gaussian. For $1 < \mu < 3$, the scaling is super-diffusive (i.e. the search pattern is tailored to minimize the distance traveled whilst locating prey), while the value $\mu = 2$ corresponds to the lower extreme of super-diffusive processes, that is a Lévy flight. For constant-velocity Lévy walks, $\zeta(2) = 2$ for $\mu < 2$ and more generally $\zeta(q) = q$ for $\mu < 2$, while $\zeta(2) = 4 - \mu$ for $2 < \mu < 3$. However, the intermittent velocities of copepods range from very likely slow steps to rare and extremely rapid displacements (Fig. 5(c)) which are incompatible with a constant-velocity Lévy walk. The velocity need not to be a constant, in which case the behavior of the function $\zeta(q)$ has yet to be defined [113]. For fractional Lévy motion (i.e. a fractional integration of order h of a Lévy noise [166]), the function $\zeta(q)$ is also bilinear with $\zeta(q) = q[h - 1 + (1/\mu - 1)]$ for $q < \mu - 1$ and $\zeta(q) = q(h - 1) + 1$ for $q \geq \mu - 1$ [167]. Finally, when the function $\zeta(q)$ is nonlinear and convex, the resulting diffusion is referred to as being multifractal [47–49], hence the term multifractal anomalous diffusion, or *multifractal random walk* [160]; see Ref. [113] for further references and explanations. The significativity of the differences between the empirical values of the function $\zeta(q)$ and their theoretical expectations for ballistic and Brownian motion, $\zeta(q) = q$ and $\zeta(q) = q/2$, can be inferred using a modified t-test [147]. Similarly, empirical $\zeta(q)$ can be practically compared using standard t- and F-tests [147].

6.3. Multifractals and zooplankton behavioral ecology so far

The applicability of Eq. (12) to zooplankton swimming behavior has initially been explored in the calanoid copepod *T. longicornis* [159,160] and the cladoceran *D. pulex* [159], which both move following a multifractal random walk (Fig. 8). These early studies were followed by investigations of the sex-specific differences in *P. annandalei* motion behavior in filtered water [109], the effects of animal density, volume and the use of 2D vs. 3D recording on *P. annadalei* and *E. affinis* swimming behavior [112], the role of female chemical cues in the motion behavior of *P. annandalei* males [115], the effect of both food and light on *C. sinicus* female swimming behavior [161], and the effect of a diatom toxin (2-trans, 4-trans decadienal) in the motion behavior of *P. annandalei* males, non-ovigerous females and ovigerous females [104]. More recently, Eq. (12) has been used to investigate the effect of male and female chemical cues on the swimming behavior of virgin and non-virgin males and females to infer the innate and acquired components of *E. affinis* (Fig. 9) and *T. longicornis* (Fig. 10) mating strategies [113]. Note that the motion behavior of all the copepod and cladoceran species investigated so far using Eq. (12) consistently exhibit multifractal properties [109,112,113,115,119,159–161], which suggests that this model of motion may be universal in crustacean zooplankton.

More specifically, in the absence of cues most observations indicate a super-diffusive multifractal random walk behavior (i.e. an extensive search pattern) that either converge towards Brownian motion [109,112,115,119,160] or switch towards sub-diffusive multifractal random walks (i.e. an intensive search pattern; [113]) when cue intensity is increasing (Figs. 9 and 10). While the nature of this switch is clearly sex- and species-dependent (Figs. 9 and 10), these results may be a first step towards generalizing to invertebrates an optimal search strategy, initially coined as the '*Lévy flight foraging hypothesis*' [168], which predicts that predators should adopt Lévy search strategies for locating sparsely and randomly distributed prey in resource-depleted environments, and Brownian movement where prey is abundant and probably more predictable, and has been used to explain the strategies of large marine predators searching for food; e.g. Refs. [168–171]. In addition, the sub-diffusive multifractal random walks observed in the presence of chemical cues are consistent with the multifractal distributions of ocean turbulence [66] and passive tracers such as phytoplankton [47–49,154–157] and copepods [46]; they may hence be an evolutionary adaptive behavior to the stochastic patterns of the olfactory landscape [113]. This is supported by theoretical developments showing that a multifractal random walk leads to increase male–female encounter rates by 33 to nearly 140% [113]; this stresses the adaptive value of multifractal random walks in the optimization of mate encounter
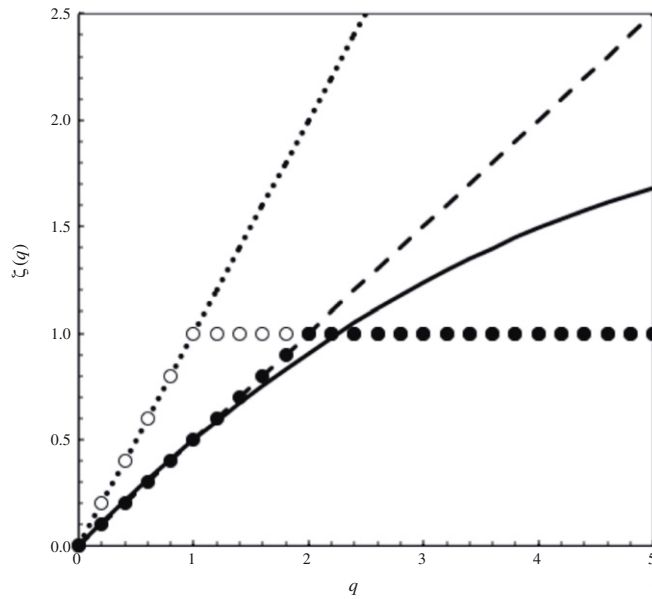
Fig. 7. Identification of a model of searching from intermittent behavioral data using the empirical function $\zeta(q)$. $\zeta(q)$ is a continuous function of the statistical order of moment q. The function $\zeta(q)$ is linear for fractional Brownian motion ($\zeta(q) = qH$), with the limit $\zeta(q) = q$ (dotted line) corresponding to ballistic motion. For Brownian motion, $\zeta(q) = q/2$ (dashed line). When $0 < H < 0.5$ the motion is sub-diffusive, while when $0.5 < H < 1$ it is super-diffusive. For Lévy flights, $\zeta(q) = q/(\mu - 1)$ for $q < \mu - 1$ and $\zeta(q) = 1$ for $q \geq \mu - 1$; μ ($1 < \mu \leq 3$) describes the tail of the probability distribution function of successive displacements l ($P(l) = kl^{-\mu}$) with $\mu = 2$ (open dots) characterizing optimal Lévy flights. The limit $\mu = 3$ is shown by black dots. For a multifractal random walk, the function $\zeta(q)$ is nonlinear and convex (continuous line).
Source: Modified from Ref. [113].
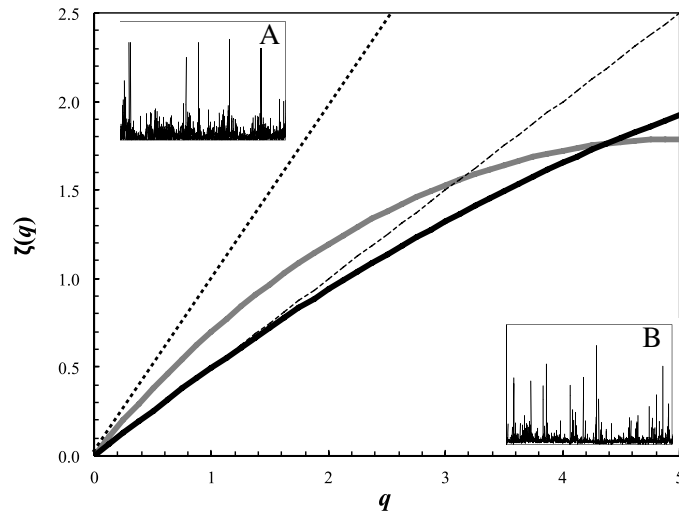
Fig. 8. Illustration of the empirical function $\zeta(q)$ obtained from 160 s of intermittent velocity fluctuations observed in *D. pulex* at 10 frames s^{-1} (A; gray curve) and *T. longicornis* at 12.5 frames s^{-1} (B; black curve). The nonlinear convex shape of $\zeta(q)$ is indicative of a multifractal random walk. The theoretical function $\zeta(q)$ expected for ballistic motion $\zeta(q) = q$ (dashed line) and Brownian motion $\zeta(q) = q/2$ (dotted line) is shown for comparison. The vertical scales are 0–6 mm s^{-1} for *D. pulex* (A) and 0–35 mm s^{-1} for *T. longicornis* (B).
Source: Modified from Ref. [159].

rate. More practically, the lack of consideration of the multifractal nature of *P. annadalei* random walk [109,112,115] in a subsequent estimate of their encounter rates may explain why encounter rates estimated from mean swimming speed of males and females are considerably lower than those reported in the literature [115].

Virgin males and females also exhibit sex-specific behaviors [113]. Specifically, in the absence of cues both *E. affinis* and *T. longicornis* virgin males exhibit diffusive swimming behavior (Figs. 9(a) and 10(a)). In contrast, virgin females of both species exhibit a multifractal random walk (Figs. 9(c) and 10(c)), suggesting that optimal search strategy is only an innate behavioral property in females of *E. affinis* and *T. longicornis*. In addition, *E. affinis* and *T. longicornis* virgin males do not exhibit any behavioral changes related to the exposure to female-conditioned water, suggesting a lack of innate behavioral
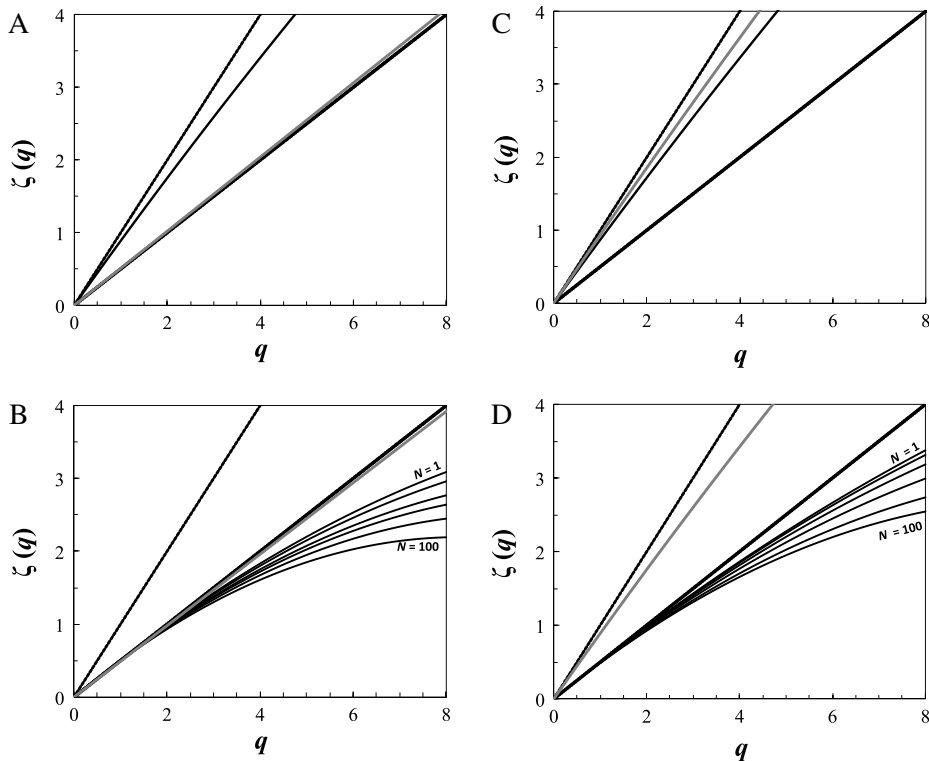
Fig. 9. Innate vs. acquired and sex-specific search strategies in both males (A, B) and non-ovigerous females (C, D) of the calanoid copepod E. affinis revealed by differences in the empirical function $\zeta(q)$ estimated in control filtered and autoclaved estuarine water (A, C) and in filtered and autoclaved estuarine water that held $N = 1$, 5, 10, 20, 50 and 100 non-ovigerous females (B) and 100 males (D) per liter during 24 h. Virgin males (A, B) and females (C, D) are shown in gray. The linear functions expected for ballistic motion ($\zeta(q) = q$; dashed line) and Brownian motion ($\zeta(q) = q/2$; dotted line) are shown for comparison.
Source: Modified from Ref. [113].

response to female pheromones. In contrast, virgin females of both species respond to male-conditioned water through a slight decrease in their multifractal super-diffusive properties (Figs. 9(c) and 10(c)), which significantly diverge from the nearly ballistic behavior exhibited under control water conditions (Figs. 9(d) and 10(d)). This indicates an innate response of females to male pheromones, and provides the first evidence for sex-specific innate adaptive behavioral properties in copepods. Further work is, however, needed to generalize the results described above to different zooplankton species and a range of environmental conditions.

Most of the studies that used Eq. (12) did not statistically assess the differences that may exist between (i) empirical $\zeta(q)$ and the theoretical functions such as ballistic motion, Brownian motion and Lévy walks [109,112,119,158–160]; (ii) empirical $\zeta(q)$ estimated under different experimental conditions, i.e. different conditions of food and light [161], conspecific individuals of different sex [109], in the presence and absence of the chemical cues of a conspecific female [112], and in the presence and absence of diatom toxin [119]; and (iii) empirical functions $\zeta(q)$ estimated from three-dimensional data and from their two dimensional (x, y), (y, z) and (x, z) projections [115,160].

In addition, apart from one exception [113], the published studies using Eq. (12) in zooplankton behavioral ecology did not quantify the value of q when empirical and theoretical $\zeta(q)$ or different empirical $\zeta(q)$ start to significantly diverge. This is, however, critical as differences in the function $\zeta(q)$ have been visually assessed [109] and statistically inferred [113] between treatments despite non-significant differences between swimming speeds. This fact further stresses the potential strength of multifractals to assess zooplankton swimming behavior especially when compared to traditional behavioral metrics. The reader is finally referred to Ref. [6] for further examples of how existing multifractal techniques such the Generalized dimension function $D(q)$, the mass exponent function $\tau(q)$ and the multifractal spectrum $f(\alpha(q))$, may be used in zooplankton behavioral ecology, and how they can be compared to the function $\zeta(q)$ described here.

7. Conclusion

Fractal and multifractal analyses – and the related fractal dimension D, exponents c and ϕ, and multifractal function $\zeta(q)$ – have the desirable properties to be independent of measurement scale and to be very sensitive to even subtle behavioral changes that may be undetectable to other behavioral variables. As early claimed by Coughlin et al. [69], this creates "*the need for fractal analysis*" in behavioral studies, which has hence the potential to become a valuable tool in zooplankton
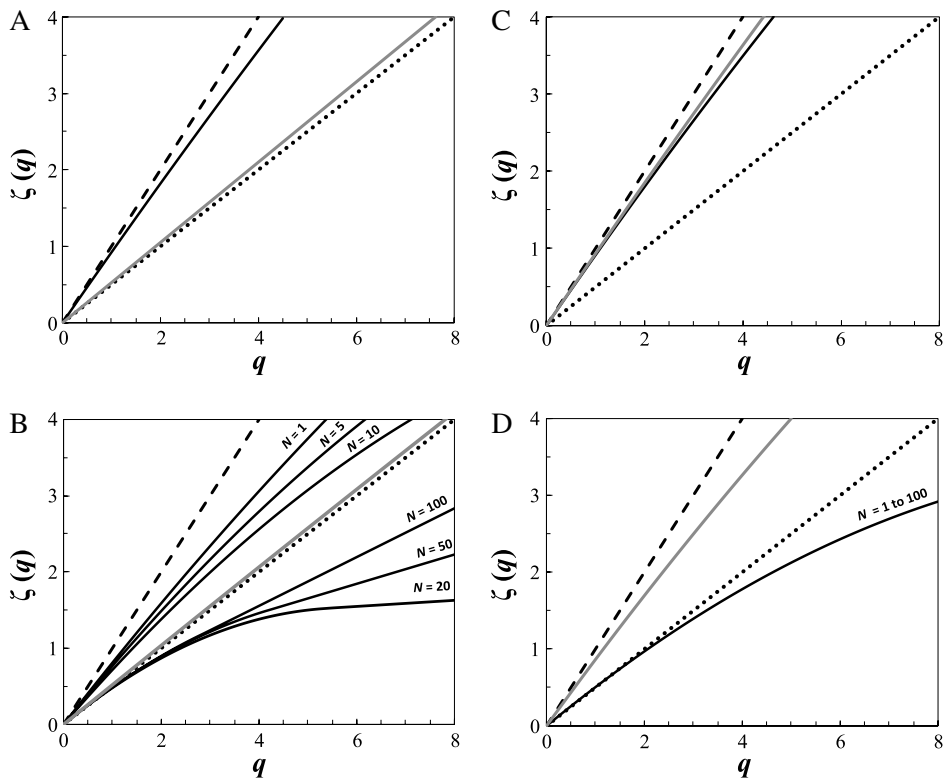
Fig. 10. Innate vs. acquired and sex-specific search strategies in both males (A, B) and non-ovigerous females (C, D) of the calanoid copepod *T. longicornis* revealed by differences in the empirical function $\zeta(q)$ estimated in control filtered and autoclaved estuarine water (A, C) and in filtered and autoclaved estuarine water that held $N = 1, 5, 10, 20, 50$ and 100 adult females (B) and 100 males (D) per liter during 24 h. Virgin males (A, B) and females (C, D) are shown in gray. The linear functions expected for ballistic motion ($\zeta(q) = q$; dashed line) and Brownian motion ($\zeta(q) = q/2$; dotted line) are shown for comparison.
Source: Modified from Ref. [113].

behavioral ecology. This is supported by the increasing use of fractals (Fig. 1(b), Tables 1–3) – and the more elaborated multifractals (Table 4) – to describe the complexity of plankton swimming behavior over the last two decades. However, as stressed in the present paper, fractal and multifractal analyses are also a risky business that may lead to irrelevant results without paying extreme attention to the critical steps addressed here and that are all likely to bias the results of any fractal or multifractal analysis. It is also noteworthy that swimming trajectories that seem distinct through visual inspections have been characterized by non-significantly different fractal dimensions [77,78]. This observation suggests that fractals may not necessarily be the ultimate tool to assess the complexity of swimming behavior under any experimental or environmental conditions, and warrants the need for further research in this area. It is hoped that this review will help in furthering the use of fractals and multifractals in zooplankton ecology in general and zooplankton behavioral ecology in particular, as it is strongly believed that our journey to further our understanding of zooplankton behavior from a fractally-colored angle is still at its early stage.

Acknowledgments

References

[1] B.B. Mandelbrot, The Fractal Geometry of Nature, Freeman, San Francisco, 1983.
[2] M.F. Barnsley, Fractals Everywhere, Morgan Kauffmann, London, 1993, 2000.

[3] E.R. Weibel, Am. J. Physiol. 261 (1991) L361.
[4] B.B. Mandelbrot, Science 156 (1967) 636.
[5] B.B. Mandelbrot, Fractals, Form, Chance, and Dimension, Freeman, San Francisco, 1977.
[6] L. Seuront, Fractals and Multifractals in Ecology and Aquatic Science, CRC Press, Boca Raton, 2010.
[7] V. Hensen, Meere 5 (1887) 1.
[8] C.M. Lalli, T.R. Parsons, Biological Oceanography. An Introduction, Elsevier, 1997.
[9] H.V. Thurman, Introductory Oceanography: Essentials of Oceanography, Prentice Hall, 1997.
[10] W.M. Durham, R. Stocker, Annu. Rev. Mar. Sci. 4 (2012) 177.
[11] R. Stocker, Science 338 (2012) 628.
[12] R. Stocker, J.R. Seymour, Microbiol. Mol. Biol. Rev. 76 (2012) 792.
[13] L. Seuront, Copepods. Diversity, Habitat and Behavior, Nova Publishers, New York, 2014.
[14] S. Frontier, in: P. Legendre, L. Legendre (Eds.), Developments in Numerical Ecology, Springer Verlag, Berlin, 1987, pp. 335–378.
[15] S. Frontier, in: M.M. Nowak (Ed.), Fractals in the Natural and Applied Sciences, Elsevier, North-Holland, 1994, pp. 119–127.
[16] R.H. Bradbury, R.E. Reichelt, Mar. Ecol. Prog. Ser. 10 (1983) 169.
[17] R.H. Bradbury, R.E. Reichelt, D.G. Green, Mar. Ecol. Prog. Ser. 14 (1984) 295.
[18] D.M. Mark, Mar. Ecol. Prog. Ser. 14 (1984) 293.
[19] J. Erlandsson, V.E. Kostylev, G.A. Williams, Ophelia 50 (1999) 215.
[20] J. Erlandsson, C.D. McQuaid, V.E. Kostylev, J. Exp. Mar. Biol. Ecol. 314 (2005) 79.
[21] V.E. Kostylev, J. Erlandsson, M.Y. Ming, G.A. Williams, Ecol. Complex. 2 (2005) 272.
[22] D.G. Zawada, J.C. Brock, J. Coast. Res. 53 (2009) 6.
[23] B. Burlando, R. Cattaneo-Vietti, R. Parodi, M. Scardi, Growth Dev. Aging 55 (1991) 161.
[24] J.A. Kaandorp, Mar. Biol. 110 (1991) 203.
[25] M. Mistri, V.U. Ceccherelli, Mar. Ecol. 14 (1993) 329.
[26] J.M. Gee, R.M. Warwick, J. Exp. Mar. Biol. Ecol. 178 (1994) 247.
[27] J.M. Gee, R.M. Warwick, Mar. Ecol. Prog. Ser. 103 (1994) 141.
[28] J. Davenport, P.J.A. Pugh, J. McKechnie, Mar. Ecol. Prog. Ser. 136 (1996) 245.
[29] J.E. Kübler, S.R. Dudgeon, J. Exp. Mar. Biol. Ecol. 207 (1996) 15.
[30] E.R. Abraham, Mar. Biol. 138 (2001) 503.
[31] J.T. Salita, W. Ekau, U. Saint-Paul, Mar. Ecol. Prog. Ser. 247 (2003) 183.
[32] J. Davenport, in: L. Seuront, P.G. Strutton (Eds.), Handbook of Scaling Methods in Aquatic Ecology. Measurement, Analysis, Simulation, CRC Press, Boca Raton, 2004, pp. 245–256.
[33] G.J. Hooper, J. Davenport, J. Mar. Biol. Assoc. UK 86 (2006) 1297.
[34] A.L. Alldredge, C. Gotschalk, Limnol. Oceanogr. 33 (1988) 339.
[35] B.E. Logan, A.L. Alldredge, Mar. Biol. 101 (1989) 443.
[36] Q. Jiang, B.E. Logan, Environ. Sci. Technol. 25 (1991) 2031.
[37] B.E. Logan, D.B. Wilkinson, Limnol. Oceanogr. 35 (1990) 130.
[38] J.R. Kilps, B.E. Logan, A.L. Alldredge, Deep-Sea Res. 41 (1994) 1159.
[39] G.A. Jackson, R. Maffione, D.K. Costello, et al., Deep-Sea Res. 44 (1997) 1739.
[40] X. Li, U. Passow, B.E. Logan, Deep-Sea Res. I 45 (1998) 115.
[41] X. Li, J.J. Zhang, J.H.W. Lee, Water Res. 38 (2004) 1305.
[42] R.G. Billiones, M.L. Tackx, M.H. Daro, Estuarine Coast. Shelf Sci. 48 (1999) 293.
[43] X. Li, B.E. Logan, Water Sci. Technol. 42 (2000) 253.
[44] F. Maggi, F. Mietta, J.C. Winterwerp, J. Hydrol. 343 (2007) 43.
[45] L. Seuront, Y. Lagadeuc, J. Mar. Ecol. Prog. Ser. 159 (1997) 81.
[46] L. Seuront, Y. Lagadeuc, J. Plankton Res. 23 (2001) 1137.
[47] L. Seuront, F. Schmitt, Y. Lagadeuc, et al., Geophys. Res. Lett. 23 (1996) 3591.
[48] L. Seuront, F. Schmitt, D. Schertzer, et al., Nonlinear Processes Geophys. 3 (1996) 236.
[49] L. Seuront, F. Schmitt, Y. Lagadeuc, et al., J. Plankton Res. 21 (1999) 877.
[50] L. Seuront, V. Gentilhomme, L. Lagadeuc, Mar. Ecol. Prog. Ser. 232 (2002) 29.
[51] M.L. Snover, J.A. Commito, J. Exp. Mar. Biol. Ecol. 223 (1998) 53.
[52] J.A. Commito, B.R. Rusignuolo, J. Exp. Mar. Biol. Ecol. 255 (2000) 133.
[53] A.I. Azovsky, M.V. Chertoprod, N.V. Kucheruk, et al., Mar. Biol. 136 (2000) 581.
[54] V. Kostylev, J. Erlandson, Mar. Biol. 139 (2001) 497.
[55] S.M. Lawrie, C.D. McQuaid, J. Exp. Mar. Biol. Ecol. 257 (2001) 135.
[56] L. Seuront, N. Spilmont, Physica A 313 (2002) 513.
[57] J. Erlandsson, C.D. McQuaid, Mar. Ecol. Prog. Ser. 267 (2004) 173.
[58] T.W. Crawford, J.A. Commito, A.M. Borowik, Landsc. Ecol. 21 (2006) 1033.
[59] J. Erlandsson, C.D. McQuaid, M. Sköld, PLoS One 6 (2011) e26958.
[60] A. Tsuda, J. Oceanogr. 51 (1995) 261–266.
[61] M. Pascual, F.A. Ascioti, H. Caswell, J. Plankton Res. 17 (1995) 1209.
[62] L. Seuront, Y. Lagadeuc, J. Plankton Res. 20 (1998) 1387.
[63] S. Lovejoy, W.J.S. Currie, M.R. Claereboudt, et al., J. Plankton Res. 23 (2001) 117.
[64] R.L. Waters, J.G. Mitchell, Mar. Ecol. Prog. Ser. 237 (2002) 51.
[65] R.L. Waters, J.R. Seymour, J.G. Mitchell, Mar. Ecol. Prog. Ser. 251 (2003) 49.
[66] H. Yamazaki, J.G. Mitchell, L. Seuront, et al., Geophys. Res. Lett. 33 (2006) L01603. http://dx.doi.org/10.1029/2005GL024103.
[67] N. Bez, S. Bertrand, Theor. Ecol. 4 (2011) 371.
[68] M.E. Lander, M.L. Logsdon, T.R. Loughlin, G.R.J. Van Blaricom, Theor. Biol. 274 (2011) 74.
[69] D.J. Coughlin, J.R. Strickler, B. Sanderson, Anim. Behav. 44 (1992) 427.
[70] L. Seuront, S. Leterme, Open Oceanogr. J. 1 (2007) 1.
[71] L. Seuront, D. Vincent, Mar. Ecol. Prog. Ser. 363 (2008) 131.
[72] L. Seuront, Physica A 309 (2011) 250.
[73] L. Seuront, Marine Ecosystems, Intech, Open Access Publisher, 2012, pp. 229–266.
[74] B.J. West, Fractal Physiology and Chaos in Medicine, World Scientific, Danvers, 2013.
[75] J.P. Sturmberg, B.J. West, in: J.P. Sturmberg, C.M. Martin (Eds.), Handbook of Systems and Complexity in Health, Springer, New York, 2013, pp. 171–192.
[76] A.J.J. MacIntosh, Primate Res. 30 (2014) 95.
[77] F.G. Michalec, M. Holzner, J.S. Hwang, S. Souissi, J. Exp. Mar. Biol. Ecol. 438 (2012) 24.
[78] R.J. Wasserman, T.J.E. Vink, J. Plankton Res. 36 (2013) 1385.
[79] D. Hamburger, O. Biham, D. Avnir, Phys. Rev. E 53 (1996) 3342.
[80] P. Turchin, Ecology 77 (1996) 2086.
[81] P. Turchin, Quantitative Analysis of Movement, Sunderland, MA, USA, 1998.

[82] D. Avnir, O. Biham, D.A. Lidar, O. Malcai, Science 279 (1997) 39.
[83] O. Malcai, D.A. Lidar, O. Biham, D. Avnir, Phys. Rev. E 56 (1997) 2817.
[84] J.M. Halley, S. Hartley, A.S. Kallimanis, et al., Ecol. Lett. 7 (2004) 254.
[85] A.M. Edwards, J. Anim. Ecol. 77 (2008) 1212.
[86] A.M. Edwards, Ecology 92 (2011) 1247.
[87] A.M. Edwards, R.A. Phillips, N.W. Watkins, et al., Nature 449 (2007) 1044.
[88] A.M. Edwards, M.P. Freeman, G.A. Breed, I.D. Jonsen, PLoS One 7 (2012) e45174. http://dx.doi.org/10.1371/journal.pone.0045174.
[89] N.A. Dowling, S.J. Hall, J.G. Mitchell, J. Fish Biol. 57 (2000) 337.
[90] N. Shimizu, C. Ogino, T. Kawanishi, Y. Hayashi, Environ. Toxicol. 17 (2002) 441.
[91] L. Seuront, M.C. Brewer, J.R. Strickler, in: L. Seuront, P.G. Strutton (Eds.), Handbook of Scaling Methods in Aquatic Ecology: Measurement, Analysis, Simulation, CRC Press, Boca Raton, 2004, pp. 333–359.
[92] L. Seuront, J.S. Hwang, L.C. Tseng, et al., Mar. Ecol. Prog. Ser. 283 (2004) 199.
[93] L. Seuront, H. Yamazaki, S. Souissi, Zool. Stud. 43 (2004) 377.
[94] M. Uttieri, E. Zambianchi, J.R. Strickler, M.G. Mazzocchi, Ecol. Model. 185 (2005) 51.
[95] L. Seuront, J. Plankton Res. 28 (2006) 805.
[96] M. Uttieri, D. Cianelli, J.R. Strickler, E. Zambianchi, J. Theoret. Biol. 247 (2007) 480.
[97] M. Uttieri, A. Nihongi, M.G. Mazzocchi, et al., J. Plankton Res. 29 (2007) 17.
[98] M. Uttieri, G.A. Paffenhöfer, M.G. Mazzocchi, Mar. Biol. 153 (2008) 925.
[99] M.S. Mahjoub, O. Anneville, J.C. Molinero, et al., Knwol. Manag. Aquat. Ecosyst. 388 (2008) 05.
[100] D. Cianelli, M. Uttieri, J.R. Strickler, E. Zambianchi, Ecol. Model. 220 (2009) 596.
[101] L. Seuront, PLoS One 6 (2011) e26283.
[102] J.J. Ziarek, A. Nihongi, N. Takeyoshi, et al., Mar. Biol. 661 (2011) 317.
[103] M.S. Mahjoub, S. Souissi, F.G. Schmitt, et al., Hydrobiologia 666 (2012) 215.
[104] F.G. Michalec, M. Holzner, D. Menu, et al., Aquat. Toxicol. 138–139 (2013) 129.
[105] L. Seuront, J. Plankton Res. 35 (2013) 724.
[106] A.J. Brooker, A.P. Shinn, S. Souissi, J.E. Bron, Parasitology 140 (2013) 756.
[107] M. Uttieri, M.G. Mazzocchi, A. Nihongi, et al., J. Plankton Res. 26 (2004) 99.
[108] F.G. Schmitt, L. Seuront, J.S. Hwang, et al., Physica A 364 (2006) 287.
[109] G. Dur, S. Souissi, F.G. Schmitt, et al., J. Plankton Res. 32 (2010) 423.
[110] F.G. Michalec, S. Souissi, G. Dur, et al., J. Plankton Res. 32 (2010) 805.
[111] K. Cailleaud, F.G. Michalec, J. Forget-Leray, et al., Aquat. Toxicol. 102 (2011) 228.
[112] G. Dur, S. Souissi, F.G. Schmitt, et al., J. Exp. Mar. Biol. Ecol. 402 (2011) 1.
[113] L. Seuront, H.E. Stanley, Proc. Natl. Acad. Sci. USA 111 (2014) 2206.
[114] A. Souissi, S. Souissi, J.S. Hwang, J. Exp. Mar. Biol. Ecol. 445 (2013) 38.
[115] G. Dur, S. Souissi, F.G. Schmitt, et al., Hydrobiologia 666 (2011) 197.
[116] M. Moison, F.G. Schmitt, S. Souissi, Aquatic Biol. 16 (2012) 149.
[117] G. Bianco, V. Botte, L. Dubroca, et al., PLoS One 8 (2013) e67640. http://dx.doi.org/10.1371/journal.pone.0067640.
[118] M. Moison, F.G. Schmitt, S. Souissi, Ecol. Res. (2013). http://dx.doi.org/10.1007/s11284-013-1034-0.
[119] F.G. Michalec, S. Kâ, M. Holzner, et al., Harmful Algae 30 (2013) 56.
[120] M.S. Mahjoub, S. Souissi, F.G. Michalec, et al., J. Plankton Res. 33 (2011) 1095.
[121] L. Sabia, M. Uttieri, F.G. Schmitt, G. Zagami, et al., Zool. Stud. 53 (2014) 49.
[122] L. Seuront, J.G. Mitchell, J. Mar. Syst. 69 (2008) 310.
[123] K.J. Falconer, The Geometry of Fractal Sets, Cambridge University Press, Cambridge, 1985.
[124] K.J. Falconer, Fractal Geometry. Mathematical Foundations and Applications, Wiley, Chichester, 1993.
[125] J. Feder, Fractals, Plenum Press, New York, 1988.
[126] H.M. Hastings, G. Sugihara, Fractals. A User's Guide for the Natural Sciences, in: Oxford Science Publications, 1993.
[127] N.C. Kenkel, D.J. Walker, Abstr. Bot. 17 (1993) 53.
[128] The British Cartographic Society, http://www.cartography.org.uk (accessed 03.03.15).
[129] N. Lesmoir-Gordon, W. Rood, R. Rodney, Introducing Fractal Geometry, Icon Books, Cambridge, UK, 2000.
[130] G. Sugihara, R.M. May, TREE 5 (1990) 79.
[131] D.H.L. Chan, B.K.K. Chan, Mar. Biol. 146 (2005) 695–705.
[132] J. Bascompte, C. Vilà, Landsc. Ecol. 12 (1997) 213.
[133] Y. Tanaka, in: L. Seuront (Ed.), Copepods: Diversity, Habitats and Behavior, Nova Publishers, New York, 2014, pp. 145–156.
[134] J.B.S. Haldane, On Being the Right Size, Oxford University Press, London, 1928.
[135] A.W. Thompson, On Growth and Form, Cambridge University Press, 1992.
[136] K. Schmidt-Nielsen, How Animals Work, Cambridge University Press, 1972.
[137] J.T. Bonner, Why Size Matters: From Bacteria to Blue Whales, Princeton University Press, 2006.
[138] B. Cox, Wonders of Life, Collins, 2013.
[139] T.H. Huxley, Biogenesis and abiogenesis, in: Collected Essays. Vol. 8, 1870, p. 229.
[140] M.W. Palmer, Vegetatio 75 (1988) 91.
[141] V.O. Nams, Landsc. Ecol. 11 (1996) 289.
[142] H. Fritz, S. Said, H. Weimerkirch, Proc. R. Soc. Lond. Ser. B 270 (2003) 1143.
[143] V.O. Nams, M. Bourgeois, Can. J. Zool. 82 (2004) 1738.
[144] V.O. Nams, Anim. Behav. 72 (2006) 1197.
[145] J.C. Russ, Fractal Surfaces, Plenum Press, New York, 1994.
[146] A.J.J. MacIntosh, L. Pelletier, A. Chiaradia, et al., Sci. Rep. 3 (2013) 1884.
[147] J.H. Zar, Biostatistical Analysis, Prentice-Hall, Englewood Cliffs, NJ, 2000.
[148] J. Erlandsson, V.E. Kostylev, Mar. Biol. 122 (1995) 87.
[149] S. Benhamou, J. Theoret. Biol. 229 (2004) 209.
[150] Y.P. Papastamatiou, P.A. DeSalles, D.J. McCauley, Mar. Ecol. Prog. Ser. 456 (2012) 233.
[151] P.M. Kareiva, N. Shigesada, Oecologia 56 (1983) 234.
[152] S. Buczkowsi, S. Kyriacos, F. Nekka, L. Carlier, Pattern Recognit. 31 (1998) 411.
[153] H.A. Eke, P.J. Bassingthwaighte, G. Raymond, et al., Pflugers Arch. 439 (2000) 403.
[154] L. Seuront, Physica A 341 (2004) 495.
[155] L. Seuront, Mar. Ecol. Prog. Ser. 302 (2005) 93.
[156] L. Seuront, Math. Model. Nat. Phenom. 3 (2008) 1.
[157] L. Seuront, F.G. Schmitt, Geophys. Res. Lett. 31 (2004) L03306. http://dx.doi.org/10.1029/2003GL018185.
[158] R.M. Montes, R.I. Perry, E.A. Pakhomov, et al., Can. J. Fish. Aquat. Sci. 69 (2012) 398.
[159] L. Seuront, F.G. Schmitt, M.C. Brewer, et al., Zool. Stud. 43 (2004) 8.
[160] F. Schmitt, L. Seuront, Physica A 301 (2001) 375.
[161] M.R. Chen, M. Moison, J.C. Molinero, J.S. Hwang, J. Exp. Mar. Biol. Ecol. 422–423 (2012) 14.

[162] A.W. Visser, T. Kiørboe, Oecologia 148 (2006) 538.
[163] G.M. Viswanathan, M.G.E. da Luz, E.P. Raposo, H.E. Stanley, The Physics of Foraging: An Introduction to Random Searches and Biological Encounters, Cambridge University Press, Cambridge, 2011.
[164] B. Mandelbrot, J.W. Van Ness, SIAM Rev. 10 (1968) 422.
[165] J.P. Bouchaud, D. Sornette, M. Potters, in: M. Dempster, S. Pliska (Eds.), Proc. Newton Institute Session on Mathematical Finance, Springer, Berlin, 1997, pp. 112–125.
[166] M. Taqqu, J. Geophys. Res. 92 (1987) 9683.
[167] F. Schmitt, D. Schertzer, S. Lovejoy, Appl. Stochastic Models Data Anal. 15 (1999) 29.
[168] G.M. Viswanathan, S.V. Buldyrev, S. Havlin, et al., Nature 401 (1999) 911.
[169] D.W. Sims, E.J. Southall, N.E. Humphries, et al., Nature 451 (2008) 1098.
[170] D.W. Sims, N.E. Humphries, R.W. Bradford, B.D. Bruce, J. Anim. Ecol. (2011). http://dx.doi.org/10.1111/j.1365-2656.2011.01914.x.
[171] N.E. Humphries, N. Queiroz, J.R.M. Dyer, et al., Nature 465 (2010) 1066.